Final Research Report

Development of New Methodologies for Deconvolution of Molecular Weight Distribution and Chemical Composition Distribution from Advanced Polyolefin Characterization Techniques

Asst. Prof. Dr. Siripon Anantawaraskul

Department of Chemical Engineering,

Faculty of Engineering, Kasetsart University

March 2011

Contract No TRG5280029

Final Research Report

Development of New Methodologies for Deconvolution of Molecular Weight Distribution and Chemical Composition Distribution from Advanced Polyolefin Characterization Techniques

Asst. Prof. Dr. Siripon Anantawaraskul

Department of Chemical Engineering,

Faculty of Engineering, Kasetsart University

This research is supported by the Thailand Research Fund.

The funding agencies may not necessary agree with the opinion presented herein.

บทคัดย่อ

เอทิลีน 1-โอลิฟินส์ โคพอลิเมอร์ ที่ผลิตด้วยระบบเร่งปฏิกิริยาที่มีหลาย site type โดยทั่วไปจะมีการกระจายตัวของน้ำหนักโมเลกุล (Molecular Weight Distribution, MWD) และการกระจายตัวขององค์ประกอบทางเคมี (Chemical composition distribution) ที่กว้าง เพราะว่าพอลิเมอร์ที่ผลิตขึ้นจากแต่ละ site type มีลักษณะโครงสร้างโมเลกุลที่แตกต่างกัน งานวิจัยนี้ ได้ศึกษาเทคนิค Simultaneous deconvolution สำหรับหาจำนวน Site type และลักษณะโครงสร้างโมเลกุลพอลิเมอร์ที่ผลิตขึ้นที่แต่ละ Site type ผลการศึกษาพบว่า การทำ Simultaneous deconvolution จากการกระจายตัวร่วมของน้ำหนักโมเลกุลและองค์ประกอบทางเคมี (Bivariate MWD and CCD) เป็นวิธีที่ดีที่สุด

ในกรณีของระบบที่เป็น 2 site type งานวิจัยที่ได้พัฒนาเกณฑ์ในการเกิดการกระจายตัวขององค์ประกอบทางเคมีที่มีสองจุดยอด โดยทดสอบเกณฑ์ที่พัฒนาขึ้นในทางทฤษฎีกับผลการจำลองและในทางการทดลองกับผลจาก เทคนิค Crystallization analysis fractionation (Crystaf) และ crystallization elution fractionation (CEF) เกณฑ์ที่เสนอขึ้นนั้นได้นำไปประยุกต์ใช้ในการศึกษาปรากฏการณ์การตกผลึกร่วมในเทคนิคทั้งสอง ผลการวิจัยพบว่าการตกผลึกร่วมที่แนวโน้มที่จะเกิดขึ้นได้มากเมื่อพอลิเมอร์ที่ผสมกันมีความสามารถในการตกผลึกคล้ายคลึงกัน เมื่อสัดส่วนของพอลิเมอร์ทั้งสองมีความแตกต่างกันอย่างมาก และเมื่ออัตราการลดอุณหภูมิสูง CEF ให้ผลการกระจายตัวขององค์ประกอบทางเคมีได้ดีกว่า CRYSTAF ด้วยระยะเวลาที่สั้นกว่า

คำสำคัญ การกระจายตัวของน้ำหนักโมเลกุล การกระจายตัวขององค์ประกอบทางเคมี พอลิเอทธิลีน crystallization analysis fractionation (Crystaf), crystallization elution fractionation (CEF), simultaneous deconvolution

Abstract

Ethylene/1-olefin copolymers produced with multiple-site-type catalytic systems typically have broad molecular weight distribution (MWD) and chemical composition distribution (CCD) because each site type produces molecules with distinct average chain microstructures. In this work, four strategies for simultaneous deconvolution of MWD and CCD were investigated to identify the number of site types and chain microstructures produced on each site type. The simultaneous deconvolution of the complete bivariate MWD and CCD was found to be the best approach to describe the complete microstructure of the model ethylene/1-butene copolymers.

In the specific case of two site-type system, a criterion for CCD bimodality was developed. The proposed criterion was validated theoretically using simulation data and experimentally using crystallization analysis fractionation (CRYSTAF) and crystallization elution fractionation (CEF) of ethylene/1-octene copolymer blends. The proposed criterion was used as a benchmark for describing cocrystallization effects in both CRYSTAF and CEF techniques. Our results showed that cocrystallization in both techniques is more prevalent when the copolymer blend has components with similar crystallizabilities, one of the components is present in much higher amount, and fast cooling rates are used. CEF was found to provide better CCD estimates than CRYSTAF in a much shorter analysis time.

Keywords: chemical composition distribution (CCD), crystallization analysis fractionation (Crystaf), crystallization elution fractionation (CEF), polyethylene, simultaneous deconvolution

Contents

บทคัดย่อ	i
Abstract	ii
Contents	iii
Research summary	1
List of project outputs	3
Appendix: Reprints of International Publications	5

Research Summary

This research project can be divided into two parts. Key summaries of each part are provided below, while the detail literature review, methodology, and discussion of results of each part are given in the reprints in the appendix of this report.

Part 1: Simultaneous Deconvolution of Molecular Weight and Chemical Composition Distribution

Ethylene/1-olefin copolymers produced with multiple-site-type catalytic systems typically have broad molecular weight distribution (MWD) and chemical composition distribution (CCD) because each site type produces molecules with distinct average chain microstructures. In this work, the simultaneous deconvolution of MWD and CCD was investigated to identify the number of site types and chain microstructures produced on each site type. Four strategies based on different data sources were tested using the MWD and CCD simulated for an ethylene/1-butene copolymer made with a catalyst having five site types. Our results indicate that the simultaneous deconvolution of the complete bivariate MWD and CCD is the best approach to describe the complete microstructure of the model ethylene/1-butene copolymers. More information about this part can be found in the following reprint in the Appendix.

1. Anantawaraskul S., Bongsontia W., Soares J.B.P., Simultaneous Deconvolution of Molecular Weight Distribution and Chemical Composition Distribution of Ethylene/1-Olefin Copolymers Synthesized with Multiple-Site-Type Catalytic Systems, Macromolecular Symposia, 2009, 282:167
2. Anantawaraskul S., Bongsontia W., Soares J.B.P., Simultaneous Deconvolution of Molecular Weight and Chemical Composition Distribution of Ethylene/1-Olefin Copolymers: Strategy Validation and Comparison, in preparation for submitting to Macromolecular Chemistry and Physics

Part 2: Investigation of Chemical Composition Distribution of Binary Blends of Ethylene/1-Olefin

Ethylene/1-olefin copolymers with controlled bimodal molecular weight distributions (MWDs) and chemical composition distributions (CCDs) have improved mechanical and rheological properties. In this work, the Stockmayer's distribution was used to develop a criterion for CCD bimodality. The proposed criterion was validated theoretically using simulation data and experimentally using crystallization analysis fractionation (CRYSTAF) and crystallization elution fractionation (CEF) of ethylene/1-octene copolymer blends. The effect of mass fraction and number average molecular weight of copolymer produced with each metallocene catalyst on CCD bimodality was also examined. The proposed criterion was then used as a benchmark for describing cocrystallization effects in both CRYSTAF and CEF techniques.

Cocrystallization of chains with different compositions leads to profiles that do not truly reflect the actual CCD of the polymer. Therefore, understanding how the polymer microstructure and the analytical conditions influence copolymer cocrystallization is critical for the proper interpretation of CRYSTAF and CEF curves. We studied the effect of chain crystallizabilities, blend compositions, and cooling rates on cocrystallization during CEF and CRYSTAF analysis. Cocrystallization is more prevalent when the copolymer blend has components with similar crystallizabilities, one of the components is present in much higher amount, and fast cooling rates are used. CEF was found to provide better CCD estimates than CRYSTAF in a much shorter analysis time. More information about this part can be found in the following reprint in the Appendix.

1. Narkchamnan K., Anantawaraskul S., Soares J.B.P., Bimodality Criterion for the Chemical Composition Distribution of Ethylene/1-Olefin Copolymers: Theoretical Development and Experimental Validation, Accepted for publication in Macromolecular Reaction Engineering
2. Suriya K., Anantawaraskul S., Soares J.B.P., Cocrystallization of Ethylene/1-Octene Copolymer Blends during Crystallization Analysis Fractionation and Crystallization Elution Fractionation, Accepted for publication in Journal of Polymer Science Part B Polymer Physics

List of Project Outputs

International Publication

1. Anantawaraskul S., Bongsontia W., Soares J.B.P., Simultaneous Deconvolution of Molecular Weight Distribution and Chemical Composition Distribution of Ethylene/1-Olefin Copolymers Synthesized with Multiple-Site-Type Catalytic Systems, Macromolecular Symposia, 2009, 282:167
2. Narkchamnan K., Anantawaraskul S., Soares J.B.P., Bimodality Criterion for the Chemical Composition Distribution of Ethylene/1-Olefin Copolymers: Theoretical Development and Experimental Validation, Accepted for publication in Macromolecular Reaction Engineering
3. Suriya K., Anantawaraskul S., Soares J.B.P., Cocrystallization of Ethylene/1-Octene Copolymer Blends during Crystallization Analysis Fractionation and Crystallization Elution Fractionation, Accepted for publication in Journal of Polymer Science Part B Polymer Physics
4. Anantawaraskul S., Bongsontia W., Soares J.B.P., Simultaneous Deconvolution of Molecular Weight and Chemical Composition Distribution of Ethylene/1-Olefin Copolymers: Strategy Validation and Comparison, in preparation for submitting to Macromolecular Chemistry and Physics

International Conference

1. Anantawaraskul S., Narkchamnan K., Suriya K., Soares J.B.P., A Criterion for Bimodality of Chemical Composition Distribution: Application as a Benchmark for Cocrystallization Study of CRYSTAF and CEF, 3rd International Conference on Polyolefin Characterization, Shanghai, China, 7-10 November 2010
2. Narkchamnan K., Anantawaraskul S., Soares J.B.P., A Criterion for Chemical Composition Distribution Bimodality of Ethylene/1-Olefin Copolymers, 17th Regional Symposium on Chemical Engineering (RSCE2010), Bangkok, Thailand, 22-23 November 2010

3. Suriya K., Anantawaraskul S., Soares J.B.P., Cocrystallization Effect in Crystallization Analysis Fractionation and Crystallization Elution Fractionation: A Case Study of Ethylene/1-Octene Copolymer Blends, 17th Regional Symposium on Chemical Engineering (RSCE2010), Bangkok, Thailand, 22-23 November 2010
4. Anantawaraskul S., Bongsontia W., Soares J.B.P., Simultaneous Deconvolution of Molecular Weight Distribution and Chemical Composition Distribution of Polyolefins Synthesized with Multi-Site Type Catalysts, 2nd International Conference on Polyolefin Characterization, Valencia, Spain, 14-17 September 2008

Appendix: Reprints of International Publications

Simultaneous Deconvolution of Molecular Weight Distribution and Chemical Composition Distribution of Ethylene/1-Olefin Copolymers Synthesized with Multiple-Site-Type Catalytic Systems

Siripon Anantawaraskul,[*1] *Warawut Bongsontia,*[1] *João B.P. Soares*[2]

Summary: Ethylene/1-olefin copolymers synthesized with multiple-site-type catalytic systems typically exhibit broad molecular weight distribution (MWD) and chemical composition distribution (CCD). These microstrucral characteristics can be described by the presence of several active site types, each of which produces chains with distinct chain microstructures. In this work, a new approach to identify the number of active site types and chain microstructures produced on each active site type was developed based on simultaneous deconvolution of the bivariate MWD/CCD information. Chain microstructures produced on each active site type are assumed to follow Stockmayer's bivariate distribution. The proposed approach was validated with simulated data of model ethylene/1-butene and ethylene/1-octene copolymers.

Keywords: chemical composition distribution; modeling; molecular weight distribution; polyethylene

Introduction

Ethylene/1-olefin copolymers synthesized with multiple-site-type catalytic systems (*i.e.*, systems with multiple-site-type catalysts, mixed catalysts, or hybrid catalysts) typically exhibit broad molecular weight distribution (MWD) and chemical composition distribution (CCD). These microstrucral characteristics can be described by the presence of several active site types, each with a different set of polymerization kinetic parameters, producing chains with distinct microstructures. Ethylene/1-olefin copolymers made with these systems can be considered a mixture, at the molecular level, of chains with various molecular weights (MW) and comonomer contents (CC) produced from all active site types.

To identify the number of active site types and chain microstructures produced on them, deconvolution of MWD obtained from gel permeation chromatography (GPC)[1–5] and deconvolution of CCD obtained from temperature rising elusion fractionation (TREF) or crystallization analysis fractionation (Crystaf)[6,7] have been investigated. The deconvolution of CCD was often performed implicitly by deconvolution of TREF or Crystaf profiles without calibration. Moreover, differences in the estimated number of active site types and mass fractions of polymers produced on each active site type may result when MWD and CCD of the same sample are deconvoluted separately.[6] Therefore, a new strategy is required to yield consistent results.

Recent advances in polyolefin characterization can help provide a great wealth of information on chain microstructures. The new developments include automated full cross-fractionation techniques (cross-fractionation by GPC/TREF or TREF/GPC which describe the interrelationship

[1] Department of Chemical Engineering, Kasetsart University 50 Phaholyothin Rd, Jatujak, Bangkok, Thailand 10900
Fax: 00662 561-4621; E-mail: fengsia@ku.ac.th
[2] Department of Chemical Engineering, University of Waterloo, Waterloo, Ontario, Canada N2L 3G1, USA

between MW and CC, known as the bivariate MWD/CCD).[8,9] The simultaneous deconvolution of such detailed information may lead to more accurate and consistent results compared to the ones obtained from separated deconvolution.[10,11]

The objective of this work is to develop a new approach for the simultaneous deconvolution of the bivariate MWD/CCD in order to determine a consistent number of active site types and chain microstructures produced on each active site type. Chain microstructures produced on each site type are assumed to follow Stockmayer's bivariate distribution. The proposed approach was validated with simulated data of ethylene/1-octene and ethylene/1-butene copolymers.

Mathematical Modeling

Microstructures of Polymer Chains Produced on Each Active Site Type

The bivariate MWD/CCD of copolymers produced on each active site type is assumed to follow Stockmayer's bivariate distribution, which is an analytical expression describing the weight distribution of kinetic chain lengths (r) and chemical compositions (F_1) for linear binary copolymers.[12,13] This distribution efficiently quantifies the distributions of molecular weight and comonomer composition due to the statistical nature of copolymerization. Stockmayer's distribution for linear binary copolymers made on each active site type is expressed as follows,

$$w(r,F_1) = r\cdot\tau^2\cdot\exp(-r\cdot\tau)\cdot\frac{1}{\sqrt{2\pi\beta/r}}\cdot\exp\left[-\frac{(F_1-\overline{F_1})^2}{2\beta/r}\right] \quad (1)$$

$$\beta = \overline{F_1}\cdot(1-\overline{F_1})\cdot\sqrt{1+4\cdot\overline{F_1}\cdot(1-\overline{F_1})\cdot(r_1\cdot r_2-1)} \quad (2)$$

where $\overline{F_1}$ is the average mole fraction of monomer type 1 in the copolymer (as calculated by the Mayo-Lewis equation), r is the kinetic chain length, r_1 and r_2 are the reactivity ratios for copolymerization ($r_1\cdot r_2=1$ for random copolymers), and $($ is the ratio of the sum of all transfer rates to the propagation rate. Note that the number average chain length is given by $1/\tau$ and, therefore, the number average molecular weight (M_n) can be calculated as $M_n = M_{repeating\ unit}/\tau.$, where $M_{repeating\ unit}$ is the average molar mass of the repeating unit in the copolymer chains.

The MWD component of Stockmayer's distribution (Flory's most probable distribution), can be obtained by integrating Stockmayer's distribution over all chemical compositions:

$$w(r) = r\cdot\tau^2\cdot\exp(-r\cdot\tau) \quad (3)$$

Similarly, the CCD component of Stockmayer's distribution can be obtained by integrating Stockmayer's distribution over all chain lengths:

$$w(F_1) = \frac{3}{4\sqrt{2\beta\tau}\left[1+\frac{(F_1-\overline{F_1})^2}{2\beta\tau}\right]^{5/2}} \quad (4)$$

Microstructures of Polymer Chains Produced with Multiple-Site-Type Catalytic Systems

Polymer chain microstructures produced with multiple-site-type catalytic systems can be considered a mixture of polymer chain microstructures produced on each active site type. Therefore, the bivariate MWD/CCD can be calculated from a superposition of Stockmayer's distributions,

$$w(r,F_1) = \sum_{i=1}^{n} m_i w_i(r,F_1) \quad (5)$$

where n is the number of active site types, m_i is the mass fraction of polymers produced on site type i, and $w_i(r, F_1)$ is the weight distribution function of polymers produced on site type i.

Similarly, the MWD and CCD of polymers produced with multiple-site-type catalytic systems can be obtained with the expressions:

$$w(r) = \sum_{i=1}^{n} m_i w_i(r) \quad (6)$$

$$w(F_1) = \sum_{i=1}^{n} m_i w_i(F_1) \quad (7)$$

where $w_i(r)$ and $w_i(F_1)$ are the MWD and CCD of copolymers produced on site type i, respectively.

Deconvolution Procedure

Theoretically, deconvolution of any weight distribution functions (Equations (5), (6), or (7)) should yield the same set of mass fractions and kinetic parameters. However, separated deconvolutions of MWD and CCD were reported to lead to slightly different results, which is not surprising given that the analytical errors in GPC, TREF and Crystaf are not the same.[6] In this work, a simultaneous deconvolution approach is proposed to obtain a more consistent set of model parameters that can describe the MWD and CCD of polyolefins. This approach should be easily applicable as the bivariate MWD/CCD information required can be obtained experimentally using automated full cross-fractionation (cross-fractionation by GPC/TREF or TREF/GPC)

To perform the deconvolution, the following procedure was used. The calculation was started by assuming that the number of active site types was 2. Simultaneous deconvolution of the bivariate MWD/CCD was performed by matching the experimental data with a superposition of Stockmayer's distribution from all active site type. The objective function (*i.e.*, the sum of the squares of differences between experimental profiles and model predictions) to be minimized is,

$$\text{Objective function} = \sum_{F} \sum_{r} [w_{\exp}(r, F_1) - w_{sim}(r, F_1)]^2 \quad (8)$$

where $w_{sim}(r, F_1)$ can be calculated with Equation (5). The mass fraction and kinetic parameters for each active site type is estimated and the value of the objective function was recorded. For n active site types, $4n$-1 parameters must be estimated (4 parameters per site, m, $\overline{F_1}$, β, and τ and $\sum_{i=1}^{n} m_i = 1$).

The number of active site types is then gradually increased and the calculation repeated until the value of the objective function stops decreasing with increasing the number of site types.

Validation of Proposed Simultaneous Deconvolution Approach

In order to validate the proposed simultaneous deconvolution approach, simulated data of a model ethylene/1-butene copolymers with five active site types and a model ethylene/1-octene copolymers with four active site types were used. The mass fractions of polymers produced on each site type and the kinetic parameters of each site type for both copolymers are summarized in Table 1 and 2. Note that, in this study, F_1 represents the mole fraction of ethylene in the copolymer. The simulated chain microstructures of both model copolymer samples are shown in Figure 1 and 2.

Table 1.
Model parameters for the model ethylene/1-butene copolymer.

Model parameters	Active site type				
	1	2	3	4	5
m	0.0160	0.2300	0.4000	0.2000	0.1540
$\overline{F_1}$	0.8838	0.9208	0.9500	0.9795	0.9841
β	0.0087	0.1427	0.3461	0.1177	0.1397
M_n	3,960	12,700	32,000	72,800	181,000

Table 2.
Model parameters for the model ethylene/1-octene copolymer.

Model parameters	Active site type			
	1	2	3	4
m	0.2790	0.3730	0.2290	0.1190
$\overline{r_1}$	0.9701	0.9907	0.9931	0.9959
β	0.2324	0.0447	0.0398	0.0437
M_n	56,561	122,322	302,387	735,595

Results and Discussion

Simultaneous deconvolution results of both model ethylene/1-butene and ethylene/1-octene copolymers are shown in Figure 3 and 4. By comparing Figure 3 with Figure 1a and Figure 4 with Figure 2a, it can be observed that two active site types cannot describe the bivariate MWD/CCD of model samples adequately. As the number of site types increases, the agreement between predictions and the ''experimental'' bivariate MWD/CCD increases. The parameters estimated for both model samples using a different number of active site types are summarized in Table 3 and 4.

The ''optimum'' number of active site types needed to describe the bivariate MWD/CCD can be determined by observing how the value of the objective function varies when the number of active site types is increased, as shown in Table 5 and 6. The sum of squares of the deviation between predictions and the model ''experimental'' value decreases significantly with the addition

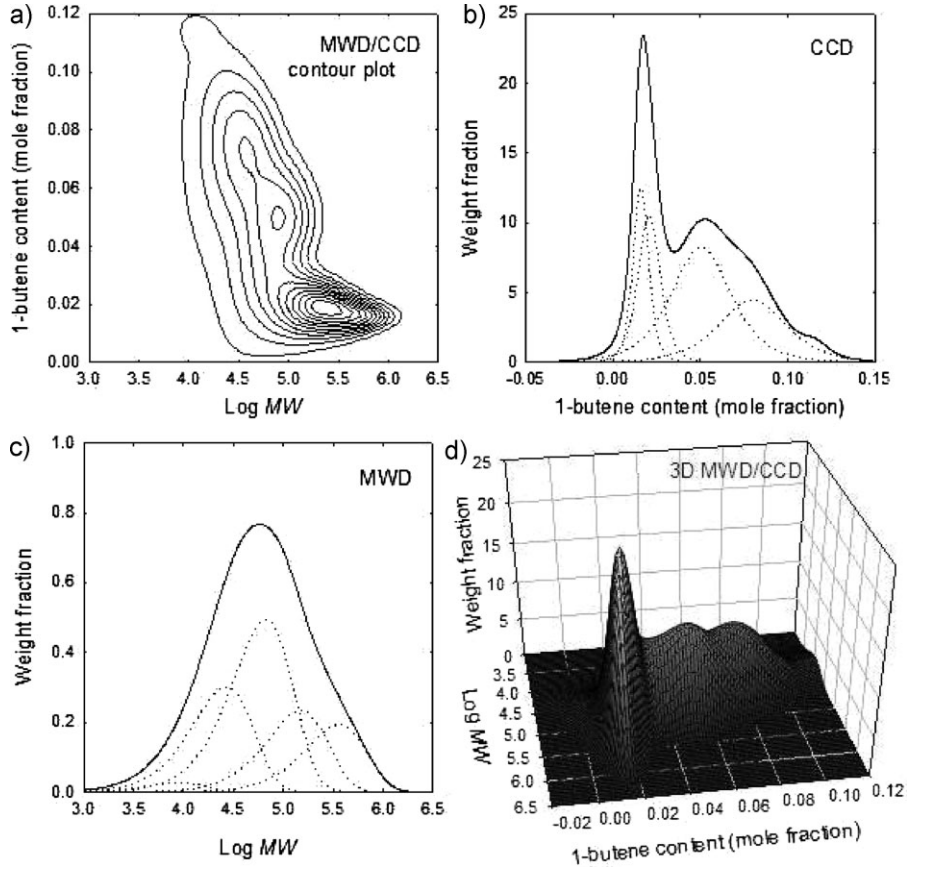

Figure 1.
Chain microstructures of a model ethylene/1-butene copolymer: (a) MWD/CCD contour plot, (b) CCD, (c) MWD, and (d) MWD/CCD.

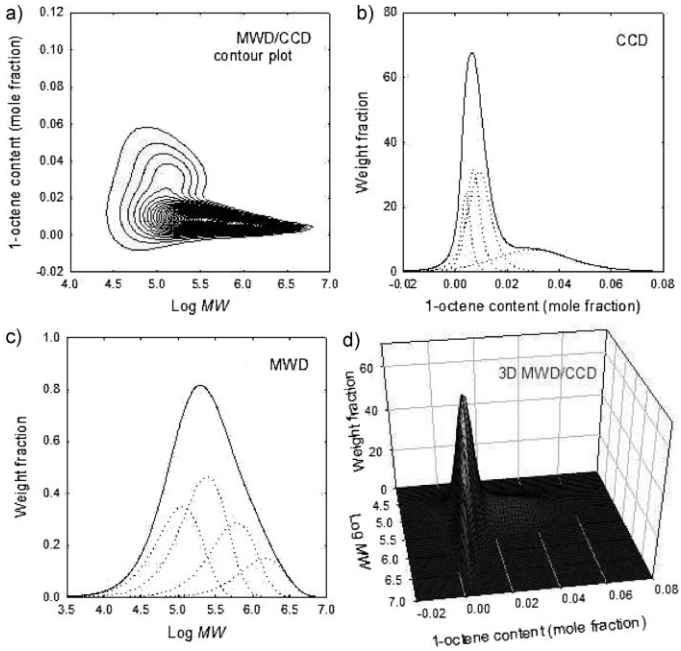

Figure 2.
Chain microstructures of a model ethylene/1-octene copolymer: (a) MWD/CCD contour plot, (b) CCD, (c) MWD, and (d) MWD/CCD.

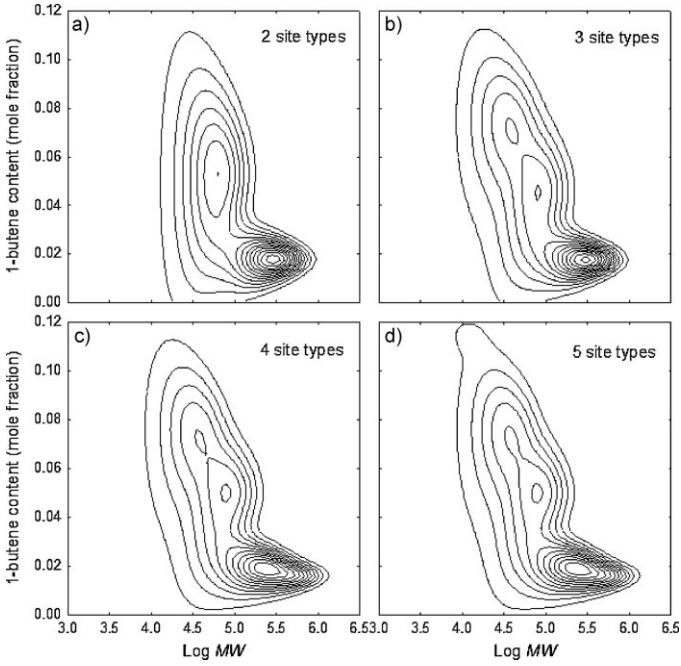

Figure 3.
Deconvolution of a model ethylene/1-butene copolymer using a different number of site types: (a) 2, (b) 3, (c) 4, and (d) 5.

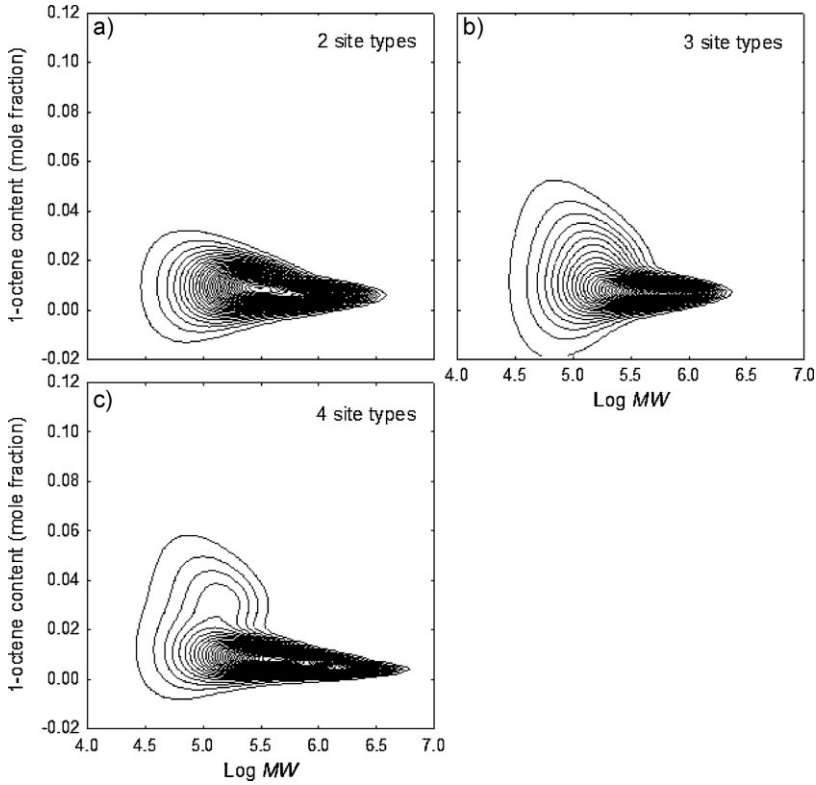

Figure 4.
Deconvolution of a model ethylene/1-octene copolymer using a different number of site types: (a) 2, (b) 3, and (c) 4.

Table 3.
Summary of model parameters for the simultaneous deconvolution of the bivariate MWD/CCD of a model ethylene/1-butene copolymer.

Parameters	Active site type				
	1	2	3	4	5
2 site types					
m	0.683000	0.317000			
$\overline{F_1}$	0.946655	0.982165			
β	1.152648	0.321425			
M_n	24,946	116,378			
3 site types					
m	0.238562	0.473654	0.287784		
$\overline{F_1}$	0.922503	0.953653	0.982364		
β	0.284059	0.972162	0.279254		
M_n	12,112	32,666	120,341		
4 site types					
m	0.239864	0.406473	0.200236	0.153427	
$\overline{F_1}$	0.920499	0.949916	0.979517	0.984092	
β	0.275411	0.666501	0.229042	0.274423	
M_n	12,281	32,042	73,290	181,671	
5 site types					
m	0.016000	0.230000	0.400000	0.200000	0.154000
$\overline{F_1}$	0.883796	0.920827	0.950019	0.979482	0.984077
β	0.014626	0.254063	0.642755	0.228368	0.272882
M_n	3,960	12,700	32,000	72,800	181,000

Table 4.
Summary of model parameters for the simultaneous deconvolution of the bivariate MWD/CCD of a model ethylene/1-octene copolymer.

Parameters	Active site type			
	1	2	3	4
2 site types				
m	0.636000	0.364000		
$\overline{F_1}$	0.990233	0.994167		
β	0.341577	0.282844		
M_n	103,190	413,244		
3 site types				
m	0.341205	0.329025	0.329771	
$\overline{F_1}$	0.983455	0.992978	0.913425	
β	1.041264	0.202136	0.000185	
M_n	66,889	248,082	452,153	
4 site types				
m	0.279000	0.373000	0.229000	0.119000
$\overline{F_1}$	0.970050	0.990690	0.993060	0.995940
β	0.833835	0.172853	0.154990	0.172088
M_n	56,561	122,322	302,387	735,595

of active site type when additional site types are necessary to improve the fitting; however, it will change little or even increase when redundant active site types are added, which lead to redundant parameters and over fit model. For the two cases investigated herein, the number of active site types could be easily and correctly determined, i.e., 5 active site types for an ethylene/1-butene copolymer and 4 active site types for an ethylene/1-octene copolymer.

From both case studies, it is clear that the proposed simultaneous deconvolution approach is very effective for identifying the number of active site types and chain microstructural parameters for each site used to produce the model copolymer. This approach can be extended to experimental resins to investigate the influence of operation parameters on chain microstructures produced on each active site type, help better quantify the main characteristics of multiple-site catalysts, and led to a better control of polymer properties made by these systems.

Table 5.
Value of the objective function as a function of the number of active site types for a model ethylene/1-butene copolymer.

Number of active site types	Objective Function Equation (8)
2	7.61×10^{-1}
3	2.19×10^{-1}
4	9.61×10^{-3}
5	2.90×10^{-6}
6	2.75×10^{-5}

Table 6.
Value of the objective function as a function of the number of active site types for a model ethylene/1-octene copolymer.

Number of active site types	Objective Function Equation (8)
2	4.43×10^{-3}
3	2.09×10^{-3}
4	1.26×10^{-13}
5	3.53×10^{-4}

Conclusion

A new approach for identifying the number of active site types and polymer chain microstructural parameters produced on each active site type for ethylene/1-olefin copolymers synthesized with multiple-site-type catalytic systems was proposed. This approach is based on the simultaneous deconvolution of the bivariate MWD/CCD, which can be obtained experimentally using GPC/TREF or TREF/GPC cross-fractionation techniques. The proposed approach

was validated with model ethylene/1-butene and ethylene/1-octene copolymers, and showed to correctly recover the parameters used in the construction of the bivariate MWD/CCD of the model polymers.

Acknowledgements: Siripon Anantawaraskul thanks financial supports from the Thailand Research Fund (TRF) and Center of Excellence for Petroleum, Petrochemicals and Advanced Materials (PPAM).

[1] J. B. P. Soares, A. E. Hamielec, *Polymer* **1995**, *36*, 2257.
[2] J. B. P. Soares, *Polym React Eng.* **1998**, *6*, 225.
[3] J. B. P. Soares, R. F. Abbott, J. N. Willis, X. Liu, *Macromol Chem Phys.* **1996**, *197*, 3383.
[4] D. E. Thompson, K. B. McAuley, P. J. McLellan, *Macromol React Eng.* **2007**, *1*, 523.
[5] D. E. Thompson, K. B. McAuley, P. J. McLellan, *Macromol React Eng.* **2007**, *1*, 264.
[6] A. A. Da Silva Filho, J. B. P. Soares, G. B. de Galland, *Macromol Chem Phys.* **2000**, *201*, 1226.
[7] A. Faldi, J. B. P. Soares, *Polymer* **2001**, *42*, 3057.
[8] A. Ortin, B. Monrabal, J. Sancho-Tello, *Macromol Symp.* **2007**, *257*, 13.
[9] W. W. Yau, *Macromol Symp.* **2007**, *257*, 29.
[10] A. A. Alghyamah, J. B. P. Soares, *Macromol. Rapid Commun.*, submitted.
[11] A. A. Alghyamah, J. B. P. Soares, *Macromol. Symp.*, submitted.
[12] W. H. Stockmayer, *J Chem Phys.* **1945**, *13*, 199.
[13] R. Simha, H. Branson, *J Chem Phys.* **1944**, *12*, 253.

Cocrystallization of Ethylene/1-Octene Copolymer Blends During Crystallization Analysis Fractionation and Crystallization Elution Fractionation

Kanokpon Suriya,[1] Siripon Anantawaraskul,[1,2] João B. P. Soares[3]

[1]Center of Excellence for Petroleum, Petrochemicals and Advanced Materials (PPAM), Department of Chemical Engineering, Faculty of Engineering, Kasetsart University, 50 Phaholyothin Rd., Jatujak, Bangkok 10900, Thailand

[2]Center for Advanced Studies in Nanotechnology and Its Applications in Chemical, Food and Agricultural Industries, Kasetsart University, Bangkok 10900, Thailand

[3]Department of Chemical Engineering, University of Waterloo, Waterloo, Ontario, Canada N2L 3G1

Correspondence to: S. Anantawaraskul (E-mail: fengsia@ku.ac.th)

Received 5 January 2011; revised 7 February 2011; accepted 9 February 2011; published online
DOI: 10.1002/polb.22231

ABSTRACT: Blending of ethylene/1-octene copolymers can be used to achieve a well-controlled broad chemical composition distribution (CCD) required in several polyolefin applications. The CCD of copolymer blends can be estimated using crystallization analysis fractionation (CRYSTAF) or crystallization elution fractionation (CEF). Unfortunately, both techniques may be affected by the cocrystallization of chains with different compositions, leading to profiles that do not truly reflect the actual CCD of the polymer. Therefore, understanding how the polymer microstructure and the analytical conditions influence copolymer cocrystallization is critical for the proper interpretation of CRYSTAF and CEF curves. In this investigation, we studied the effect of chain crystallizabilities, blend compositions, and cooling rates on cocrystallization during CEF and CRYSTAF analysis. Cocrystallization is more prevalent when the copolymer blend has components with similar crystallizabilities, one of the components is present in much higher amount, and fast cooling rates are used. CEF was found to provide better CCD estimates than CRYSTAF in a much shorter analysis time. © 2011 Wiley Periodicals, Inc. J Polym Sci Part B: Polym Phys 000: 000–000, 2011

KEYWORDS: blends; cocrystallization; crystallization analysis fractionation; crystallization elution fractionation; fractionation of polymers; polyethylene

INTRODUCTION The chemical composition distribution (CCD), which describes the weight distribution of comonomer fraction in copolymers, is among the most important microstructural distributions of copolymers as it can significantly influence product properties.[1] The physical blending of copolymers is one of the possible approaches to make copolymers with well-controlled broad CCDs and desired properties.

The CCD of ethylene/1-octene copolymer blends can be estimated using crystallization analysis fractionation (CRYSTAF), which fractionates polymer chains according to chain crystallizabilities in a dilute solution.[2–6] In previous CRYSTAF studies,[7–9] cocrystallization among some blend components with different average comonomer content and/or molecular weights was found to be strong enough to distort the measured CCD and mislead its interpretation.

Recently, a novel characterization technique to estimate CCD called crystallization elution fractionation (CEF) was introduced by Monrabal.[10,11] CEF involves two fractionation steps: crystallization and elution. The crystallization step of CEF involves the continuous flow of the polymer solution through the CEF column, whereas the temperature decreases at a constant cooling rate. During this step, polymer chains will crystallize at different locations along the column according to their chain crystallizabilities. In the elution step, a pure solvent flows through the column to dissolve polymers precipitated during the crystallization step, whereas the temperature increases following a constant heating rate. The concentration of polymer solution passed through the column is monitored via dual wavelength infrared detector placed at the exit of the CEF column. CEF bears many similarities to temperature elution fractionation (TREF), with the main difference that no solvent is flowing through the column during the crystallization step in TREF.

The fractionation efficiency of CEF is greatly enhanced because the dynamic crystallization taking place under solvent flow causes the physical segregation of polymer fractions with different crystallizabilities along the axis of the column. The fractionation during the crystallization step in TREF is not as efficient because polymer fractions with different crystallizabilities practically crystallize at the same

TABLE 1 Properties of Ethylene/1-octene Copolymer Samples Used in This Investigation

Sample	Mole Percent of 1-Octene	CRYSTAF Peak Temperature (T_C, °C)[a]	CEF Peak Temperature (T_E, °C)[b]	Number Average Molecular Weight (M_n, g·mol^{-1})	Dispersity
O116	1.16	75.0	88.7	47,100	2.16
O220	2.20	66.6	82.4	47,700	2.25
O351	3.51	55.4	72.3	49,800	2.20

[a] CRYSTAF peak temperature measured at a cooling rate of 0.2 °C·min^{-1}
[b] CEF peak temperatures measured at a cooling rate of 3 °C·min^{-1}, a crystallization flow rate of 0.25 mL min^{-1}, a heating rate of 3 °C·min^{-1}, and an elution flow rate of 1 mL min^{-1}

location. Because of the superior fractionation during dynamic crystallization, the CEF analysis time can be significantly reduced, and less cocrystallization is expected. The effect of operating parameters and polymer properties on cocrystallization during CEF analysis, however, has never been quantified systematically. Understanding how these parameters influence the cocrystallization phenomenon during CEF analysis is critical to use this technique for the proper quantification of copolymer CCDs.

In this article, the effect of different chain crystallizability, blend compositions, and cooling rates on the cocrystallization of ethylene/1-octene copolymer blends during CRYSTAF and CEF analysis was investigated. Cocrystallization in CRYSTAF was used as a benchmark to evaluate how strongly it affects CEF analysis.

EXPERIMENT

Materials

Three ethylene/1-octene copolymers made with a single-site-type catalyst were kindly donated by Dow Chemical. They were selected to have different comonomer contents but similar number average molecular weights (M_n) to avoid any subtle molecular weight effect on cocrystallization. Because they were made with a single-site-type catalyst, they had narrow and unimodal molecular weight (MWDs) and CCDs. The properties of all investigated copolymers are summarized in Table 1. The first letter in the copolymer name indicates comonomer type. The three-digit numbers in the copolymer name indicate average comonomer content. For example, O116 indicates an ethylene/1-octene copolymer with 1.16 mol % of 1-octene.

Binary copolymer blends of different compositions were used to investigate cocrystallization in CRYSTAF and CEF. The compositions and properties of the blends are summarized in Table 2. The number in blend identification name indicates the CRYSTAF peak temperature difference between the two copolymers in the blend. For example, B08 is a blend in which the CRYSTAF peak temperatures for each component differ by ~8 °C (75.0 °C for O116 and 66.6 °C for O220).

CRYSTAF Analysis

CRYSTAF analysis was performed using CRYSTAF 200 (Polymer Char S.A., Valencia, Spain). 1,2,4-trichlorobenzene (TCB), which is used as a solvent for all samples, is added with an antioxidant Irganox 1010 (CIBA) at a concentration of 0.25 mg L^{-1}. In the analysis, a sample is dissolved in 1,2,4-trichlorobenzene (TCB) in a 60-mL stirred vessel at a concentration of 0.4 mg mL^{-1}. The polymer solution is held at 160 °C for 155 min to ensure the complete dissolution of the polymer. The temperature of the polymer solution is decreased to 100 °C and allowed to stabilize for 50 min before starting the fractionation. Then, the solution temperature is reduced to 30 °C under a specified constant slow cooling rate (0.05, 0.2, or 0.5 °C min^{-1}). As the polymer precipitates, the polymer concentration in solution decreases as a function of temperature and is monitored using an in-line IR detector, generating a plot of normalized polymer concentration versus temperature, often referred to as the cumulative CRYSTAF curve. The fractions of polymers crystallized at each temperature can be obtained by numerical differentiation of the cumulative curve. At a cooling rate of 0.2 °C min^{-1}, the CRYSTAF analysis time is ~12 h. However, it should be noted that up to five samples can be analyzed simultaneously.

CEF Analysis

CEF analysis was performed using CEF-21 (Polymer Char S.A., Valencia, Spain). 1,2,4-trichlorobenzene (TCB), which is

TABLE 2 Compositions of Ethylene/1-Octene Copolymer Blends Used in This Investigation

Blend Sample	Copolymer 1	Copolymer 2	Difference Between CRYSTAF Peak Temperatures (ΔT_C, °C)	Difference Between CEF Peak Temperatures (ΔT_E, °C)
B08	O116	O220	8.4	6.3
B20	O116	O351	19.6	16.4
B11	O220	O351	11.1	10.1

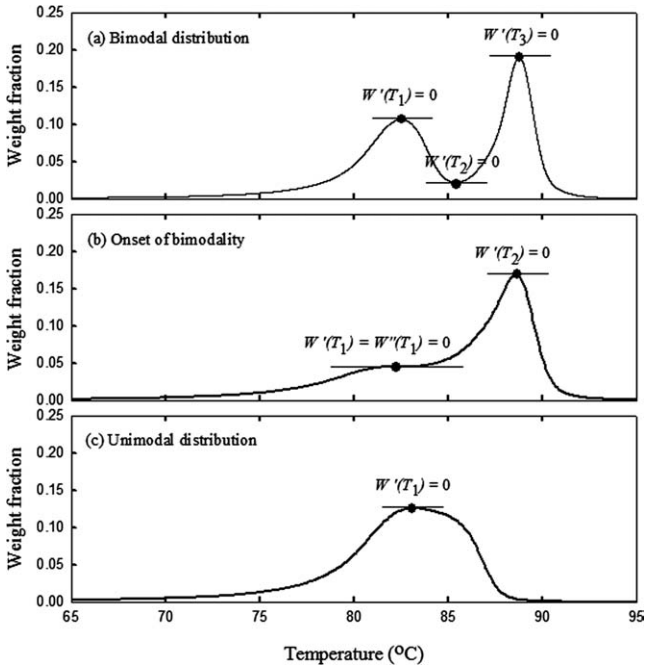

FIGURE 1 Classification of CRYSTAF and CEF profiles of binary copolymer blends (a) bimodal distribution, (b) at the onset of bimodality, and (c) unimodal distribution.

used as a solvent for all samples, is added with an antioxidant Irganox 1010 (CIBA) at a concentration of 0.25 mg L^{-1}. During the sample preparation stage, a polymer sample is dissolved in 8 mL of 1,2,4-trichlorobenzene (TCB) in a vial at a concentration of 4 mg mL^{-1} at 160 °C in the auto sampler (Polymer Char S.A., Valencia, Spain). The polymer solution is stabilized at 95 °C for 2 min before being injected in the CEF column. The crystallization step starts by decreasing the column temperature from 95 to 35 °C under a constant cooling rate and a constant crystallization flow rate. Polymer chains are crystallized and fractionated along the CEF column in this step. After the crystallization cycle is over, the column temperature is held at 35 °C for a few minutes under fresh solvent flow at a constant elution flow rate of 1 mL min^{-1}. The elution step starts when the temperature starts increasing at a constant heating rate of 3 °C·min^{-1}, from 35 to 140 °C. The concentration of polymer in the eluent is monitored as a function of the elution temperature by a dual wavelength infrared detector placed at the exit of the CEF column. The CEF analysis time is approximately an hour.

Data Analysis

Calculated CRYSTAF and CEF Profiles of the Binary Blends

Cocrystallization can be qualitatively measured by comparing the experimental and the calculated CRYSTAF and CEF profiles of copolymer blends. The CRYSTAF or CEF profiles of polymer blends in the absence of cocrystallization are given by weighted sum of the profiles for the blend components measured individually. For binary blends, this expression is shown in eq 1,[8]

$$\hat{x}(T) = m_1 x_1(T) + (1 - m_1) x_2(T) \quad (1)$$

where $\hat{x}$ represents the calculated CRYSTAF or CEF profile for the blend as a function of temperature (crystallization temperature, T_C, for CRYSTAF and elution temperature, T_E, for CEF), x_1 (T) and x_2 (T) are the profiles of blend components, measured individually, and m_1 is the mass fraction of one of the blend components, arbitrarily selected as the component with the lower comonomer content (i.e., higher crystallization temperature) in this study.

Estimation of the Cocrystallization Extent

We will classify the CRYSTAF and CEF profiles as bimodal, on the onset of bimodality, and unimodal. If the first derivative of the profile is zero at three distinct temperatures, $W'(T_1) = W'(T_2) = W'(T_3) = 0$, the profile is bimodal as shown in Figure 1(a). In this case, T_1 and T_3 are maximum points, and T_2 is the minimum point in the profile. At the onset of bimodality, Figure 1(b), the first derivative will be zero at only two temperatures, $W'(T_1) = W'(T_2) = 0$. In addition, the second derivative will be also null at the inflection point, $W''(T_1) = 0$. Finally, the first derivative will be zero only at one temperature, $W'(T_1) = 0$, for unimodal profiles, as depicted in Figure 1(c).

Unimodal profiles for polymer blends are indicative of very significant cocrystallization of the blend components, to the extent that the crystallization/elution peaks of the individual components cannot be observed separately.

If the profile is bimodal or on the onset of bimodality, the mass fraction of each component in the blend can be estimated by integrating the area under the curves for corresponding component (Fig. 2). The total area under the curve is split into two parts at the minimum or inflection point. The mass fraction estimated from this integration (m_{exp}) can be compared with the known mass fraction (m_{actual}) in the blend, and their difference can be used to quantify the extent of cocrystallization. Large deviations reflect strong cocrystallization effects.

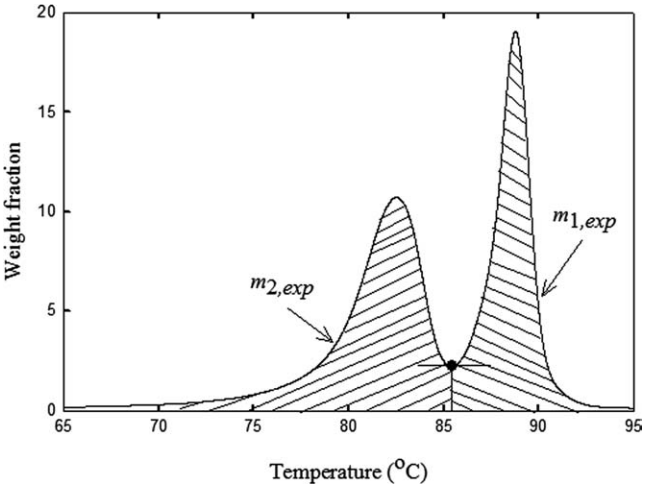

FIGURE 2 Estimation of mass fractions (m_{exp}) of blend components from areas under the curve in the case of bimodal CCD.

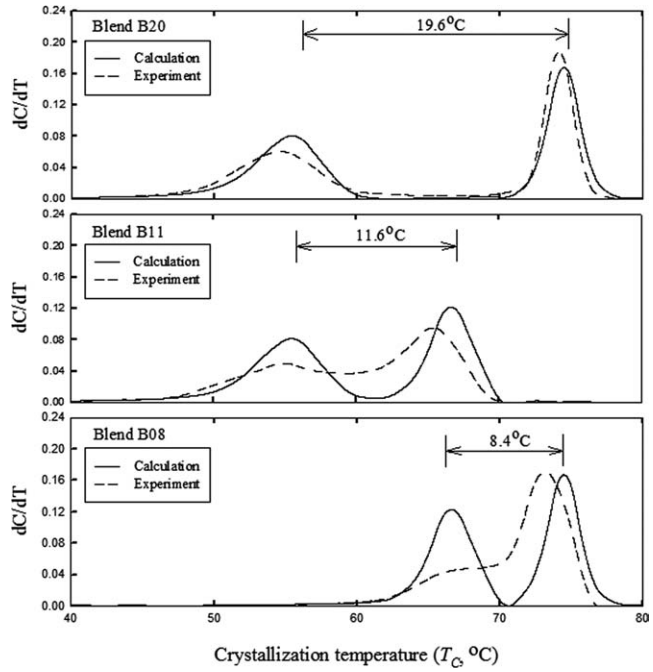

FIGURE 3 Effect of difference between CRYSTAF peak temperatures (ΔT_C) on CRYSTAF profiles of copolymer blends with a mass fraction of 0.5 at a cooling rate of 0.2 °C min^{-1}.

RESULTS AND DISCUSSION

Figures 3 and 4 show CRYSTAF and CEF profiles of the ethylene/1-octene copolymer blends listed in Table 2, respectively. Cocrystallization in CRYSTAF and CEF becomes more prominent when the difference between peak temperatures of the two components is small, that is, when the blend components have similar chain crystallizabilities. In the case of blend B08, cocrystallization is very significant, and the CRYSTAF and CEF profiles are on the onset of bimodality with a broad low temperature shoulder, very different from the bimodal distribution calculated assuming no cocrystallization.

Figure 5 shows that the blend compositions (m_{exp}) estimated from the integration of CRYSTAF and CEF profiles are gradually closer to the actual mass fractions ($m_{actual} = 0.5$) when the difference between the CRYSTAF or CEF peak temperatures (ΔT_C or ΔT_E) of individual blend components increases. As large deviations between m_{exp} and m_{actual} reflect a strong cocrystallization effect, this result is the graphical representation that similar chain crystallizabilities promote cocrystallization during CRYSTAF and CEF analysis. It also quantifies the extent of cocrystallization, indicating that for these analysis conditions, both CRYSTAF and CEF suffer from comparable cocrystallization effects.

To examine the effect of m on blend cocrystallization, B08 blends with different compositions that were prepared and analyzed by CRYSTAF and CEF (Figs. 6 and 7). The CRYSTAF and CEF profiles for $m = 0.5$ were on onset of bimodality, whereas all other blend compositions were unimodal, instead of the bimodal distributions that would be expected in the absence of cocrystallization. This indicates that cocrystallization of blend components is more likely to occur when one of the blend components is present in higher amount. This observation is in agreement with a previous cocrystallization study of polymer melts for polyolefin binary blends, where it was reported that the component with the smaller fraction tended to cocrystallize with the component with the larger fraction.[12] Polyolefin blends that have a 50/50 wt % composition tend to cocrystallize the least.

These results seem to contradict the previous work by Brull et al.,[13] which reported the CRYSTAF analysis of polyethylene and polypropylene blends. Negligible cocrystallization was reported even when blends with mass fractions of polypropylene or polyethylene as low as 5% wt. were analyzed. However, besides the fact that the chain crystallizabilities between polyethylene and polypropylene is quite large ($\Delta T_C = 34.7$ °C), their crystallite structures are also distinct, which minimizes cocrystallization between the two blend components.

Figures 8 and 9 show the effect of the cooling rate on CRYSTAF and CEF profiles of the B08 blends. Fast cooling rates promote cocrystallization, shifting the CRYSTAF and CEF profiles to lower temperatures and making them more likely to appear unimodal. Faster cooling rates will push the crystallization process farther away from equilibrium toward a purely kinetic controlled crystallization. The distortion due to kinetic controlled crystallization can be so severe that CCD of investigated blends could be misinterpreted, especially at fast cooling rates. Similar observations were also

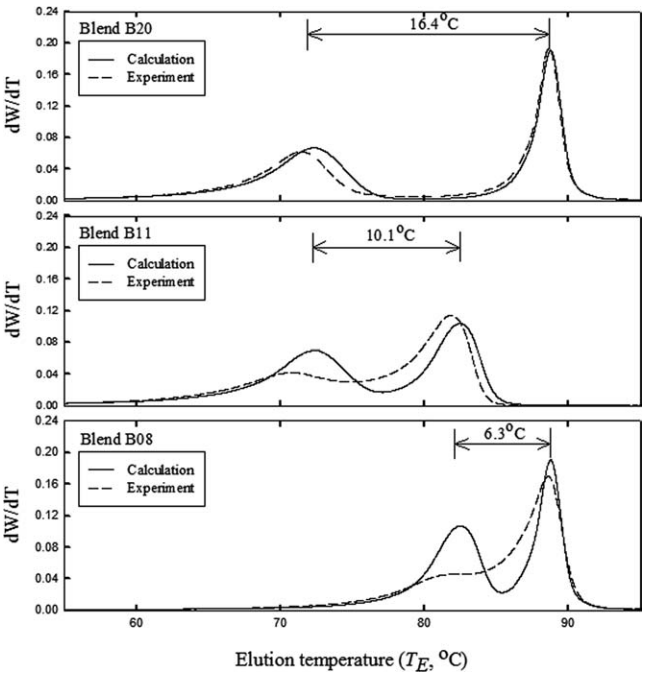

FIGURE 4 Effect of difference between CEF peak temperatures (ΔT_E) on CEF profiles of copolymer blends with a mass fraction of 0.5 at a cooling rate of 3 °C min^{-1}.

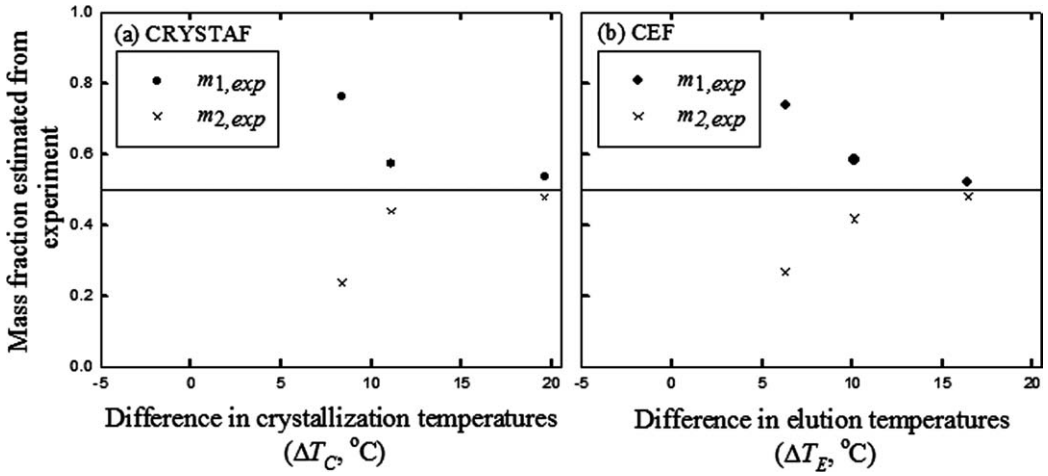

FIGURE 5 Effect of difference between peak temperatures (ΔT_C and ΔT_E) on blend compositions (m_{exp}) estimated from (a) CRYSTAF and (b) CEF profiles of copolymer blends with an actual blend composition of 0.5.

reported in the literature for CRYSTAF.[4,7–9] Our results confirm that fractionations with CRYSTAF and CEF occur at conditions that are far from thermodynamic equilibrium.

It is interesting to note that shifts in CEF peak temperature due to varying cooling rate are much less pronounced than those for CRYSTAF. In fact, CEF can detect the expected

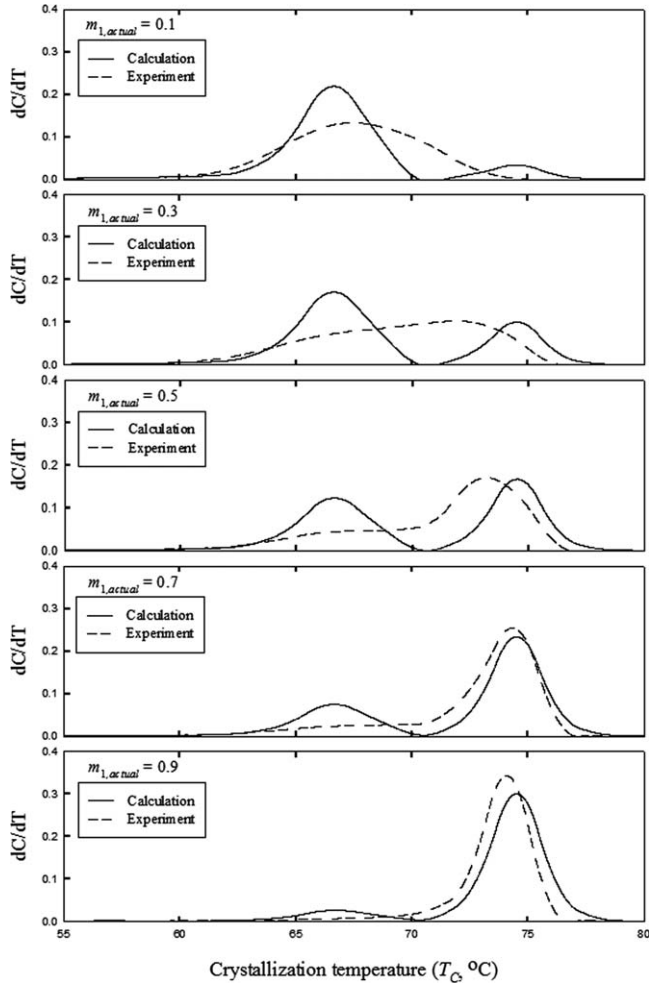

FIGURE 6 Effect of blend composition on CRYSTAF profiles of blend B08 at a cooling rate of 0.2 °C min^{-1}.

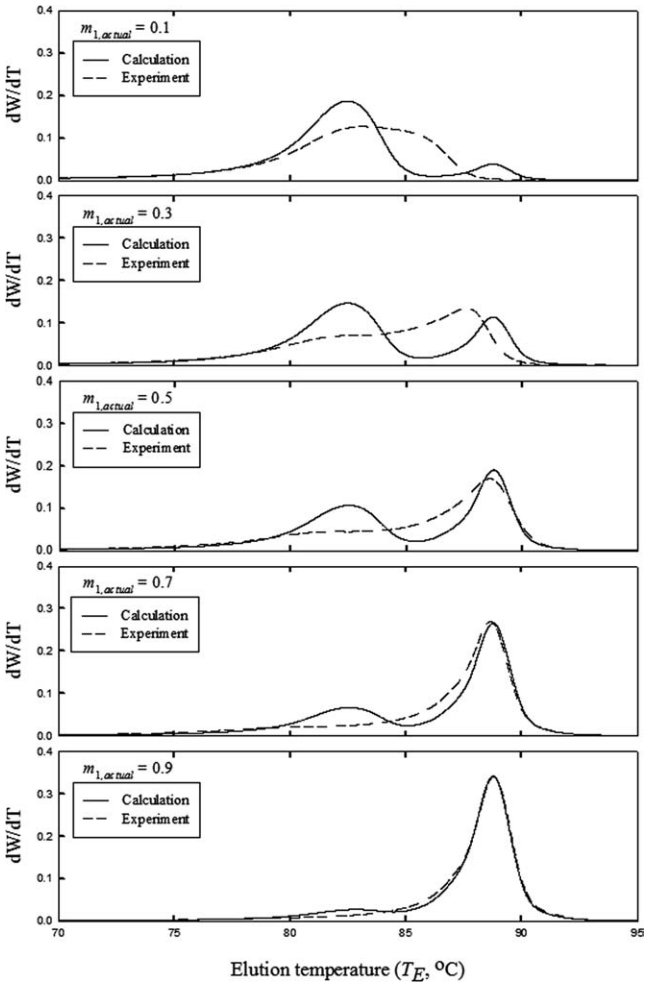

FIGURE 7 Effect of blend composition on CEF profiles of blend B08 at a cooling rate of 3 °C/min.

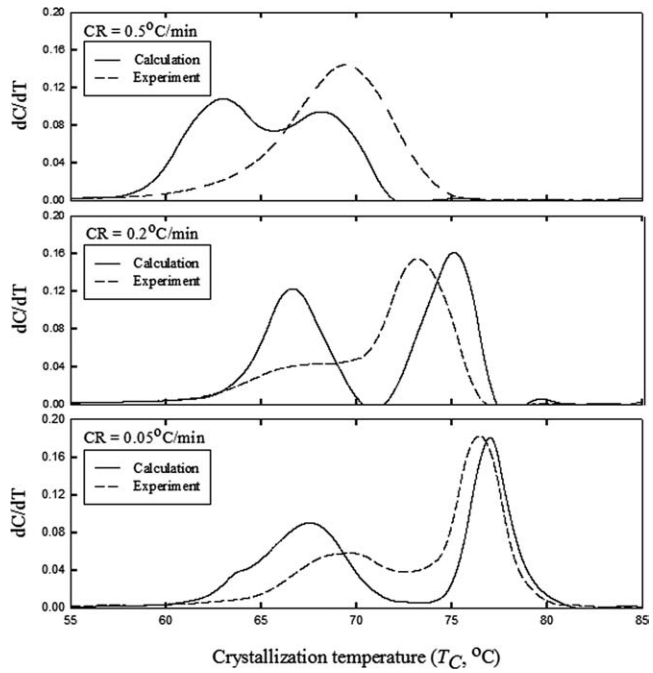

FIGURE 8 Effect of cooling rate on CRYSTAF profiles of blend B08 with a mass fraction of 0.5.

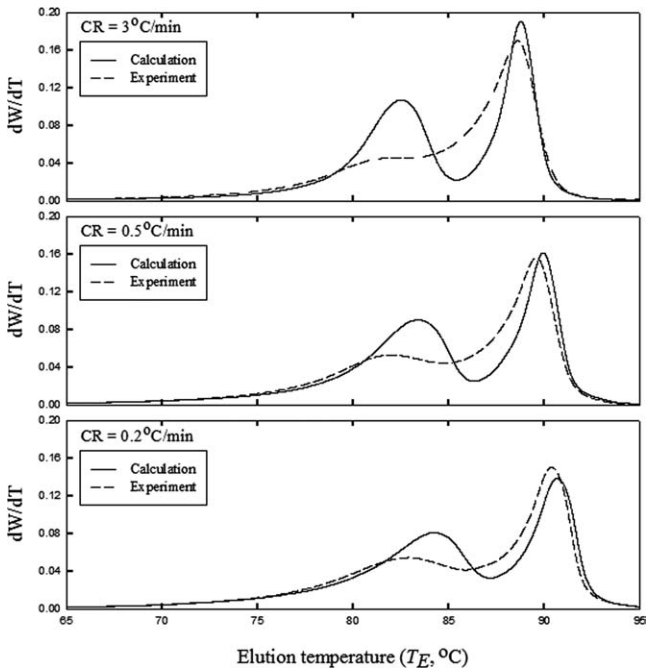

FIGURE 9 Effect of cooling rate on CEF profiles of blend B08 with a mass fraction of 0.5.

bimodal distributions much more effectively than CRYSTAF. These results confirm the advantage of CEF in term of robustness when subjected to fast cooling rates.

The cooling rate effect on cocrystallization in CRYSTAF and CEF can be better quantified by calculating the deviation between the estimated (m_{exp}) and actual blend composition ($m_{actual} = 0.5$) as shown in Figure 10. Note that the deviations for CRYSTAF can be calculated at only two cooling rates because the profile at a cooling rate of 0.5 °C min^{-1} is already completely unimodal, as shown in Figure 8.

These results provide clear evidence that a slow cooling rate greatly minimizes cocrystallization in both CRYSTAF and CEF. It can also be concluded that the extent of cocrystallization in CEF is much lower than in CRYSTAF at the same cooling rate, making CEF a much faster CCD analytical than CRYSTAF.

Although CEF is believed to provide an efficient polymer fractionation process with physical separations occurring in both dynamic crystallization and elution steps, our results show that cocrystallization may still be significant at the typically used "high-throughput" conditions. However, it should be noted that these conditions are aimed toward short analysis time, not high peak resolution. CEF analysis conditions (i.e., cooling rate, crystallization flow rate, heating rate, and elution flow rate) can be changed to minimize cocrystallization and optimize peak resolution, as will be explored in a future publication from our group. Nonetheless, even in short analysis time mode, CEF is clearly superior to CRYSTAF

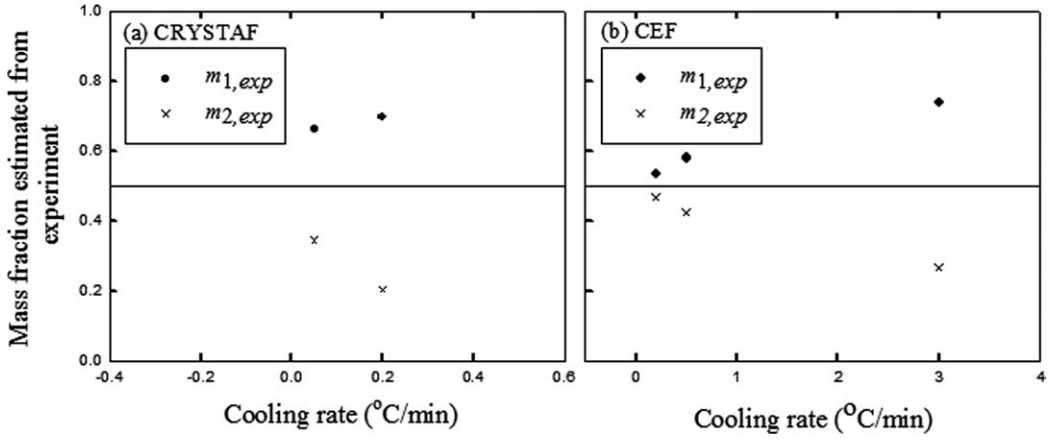

FIGURE 10 Effect of cooling rate on blend compositions ($m_{exp.}$) estimated from (a) CRYSTAF and (b) CEF profiles of blend B08 with an actual blend composition of 0.5.

because it gives results with equivalent or better resolution at much shorter analysis time.

CONCLUSIONS

The effect of chain crystallizabilities, blend composition, and cooling rate on the extent of cocrystallization in CRYSTAF and CEF were investigated. The extent of cocrystallization in both CRYSTAF and CEF increases as the chain crystallizabilities are close, one of the blend components is present in large excess, and fast cooling rates are used. However, CEF was found to be more robust and have less cocrystallization than CRYSTAF. CEF also requires much shorter analysis times for to achieve peak resolutions that are comparable with CRYSTAF and is well suited to high-throughput CCD characterization.

ACKNOWLEDGMENTS

The authors would like to thank the Dow Chemical Company for kindly donating the copolymer samples used in this investigation and the financial support from the Thailand Research Fund (TRF), Center of Excellence for Petroleum, Petrochemical and Advanced Materials (PPAM), Graduate School and Faculty of Engineering, Kasetsart University. K. Suriya would also like to thank Abdulaziz A. Alghyamah, Saeid Mehdiabadi, and Yiyoung Choi (Department of Chemical Engineering, University of Waterloo, Waterloo, ON, Canada) for their helpful discussions.

REFERENCES AND NOTES

1 Rana, D.; Kim, H. L.; Kwag, H.; Rhee, J.; Cho, K.; Woo, T.; Lee, B. H.; Choe, S. J. *Polym. Sci.* **2000,** *76*, 1950–1964.

2 Anantawaraskul, S.; Soares, J. B. P.; Wood-Adams, P. M. *Adv. Polym. Sci.* **2005,** *182*, 1–54.

3 Soares, J. B. P.; Anantawaraskul, S. *J. Polym. Sci. Part B: Polym. Phys.* **2005,** *43*, 1557–1570.

4 Sweed, M. Co-Crystallization in Polyolefin Blends Studied by Various Crystallization Analysis Techniques, Master Thesis, University of Stellenbosch, April, **2006.**

5 Monrabal, B. J. *Appl. Polym. Sci.* **1994,** *52*, 491–499.

6 Britto, L. J. D.; Soares, J. B. P.; Penlidis, A.; Monrabal, B. *J. Polym. Sci. Part B: Polym. Phys.* **1999,** *37*, 539–552.

7 Anantawaraskul, S.; Soares, J. B. P.; Wood-Adams, P. M. *J. Polym. Sci. Part B: Polym. Phys.* **2003,** *41*, 1762–1778.

8 Anantawaraskul, S.; Soares, J. B. P.; Wood-Adams, P. M. *Macromol. Chem. Phys.* **2004,** *205*, 771–777.

9 Fonseca, C. A.; Harrison, I. R. *Thermochim. Acta* **1998,** *313*, 37–41.

10 Monrabal, B.; Sancho-Tello, J.; Mayo, N.; Romero, L. *Marcromol. Symp.* **2007,** *257*, 71–79.

11 Monrabal, B.; Romero, L.; Mayo, N.; Sancho-Tello, J. *Marcromol. Symp.* **2009,** *282*, 14–24.

12 Xu, J.; Xu, X.; Chen, L.; Feng, L.; Chen, W. *Polymer* **2001,** *42*, 3867–3874.

13 Brull, R.; Grumel, V.; Pasch, H.; Raubenheimer, H. G.; Sanderson, R.; Wahner, U. M. *Macromol. Symp.* **2002,** *178*, 81–91.

Article type: Full paper

Simultaneous Deconvolution of Molecular Weight and Chemical Composition Distribution of Ethylene/1-Olefin Copolymers: Strategy Validation and Comparison

Siripon Anantawaraskul[1,2*], Warawut Bongsontia[1], João B.P. Soares[3]

W. Bongsontia, Prof. S. Anantawaraskul

[1]Center of Excellence for Petroleum, Petrochemicals and Advanced Materials (PPAM), Department of Chemical Engineering, Faculty of Engineering, Kasetsart University, 50 Phaholyothin Rd., Jatujak, Bangkok, 10900, Thailand

[*]Tel: 662-942-8555 ext. 1231, Fax: 662-561-4621, E-mail: fengsia@ku.ac.th

[2]Center for Advanced Studies in Nanotechnology and Its Applications in Chemical, Food and Agricultural Industries, Kasetsart University, Bangkok, 10900, Thailand

Prof. J. B. P. Soares

[3]Department of Chemical Engineering, University of Waterloo,

Waterloo, Ontario, N2L 3G1, Canada

Keywords: chemical composition distribution; modeling; molecular weight distribution; simultaneous deconvolution; polyethylene (PE)

Abstract

Ethylene/1-olefin copolymers produced with multiple-site-type catalytic systems typically have broad molecular weight distribution (MWD) and chemical composition distribution (CCD) because each site type produces molecules with distinct average chain microstructures. In this work, the simultaneous deconvolution of MWD and CCD was investigated to identify the number of site types and chain microstructures produced on each site type. Four strategies based on different data sources were tested using the MWD and CCD simulated for an ethylene/1-butene copolymer made with a catalyst having five site types. Our results indicate that the simultaneous deconvolution of the complete bivariate MWD and CCD is the best approach to describe the complete microstructure of the model ethylene/1-butene copolymers.

Introduction

Multiple-site-type catalysts such as heterogeneous Ziegler-Natta and Phillips catalysts, mixed metallocene catalysts, or hybrid catalysts, typically produce ethylene/1-olefin copolymers with broad molecular weight distribution (MWD) and chemical composition distribution (CCD) because each site type has a different set of polymerization kinetic parameters, producing chains with distinct average microstructural properties.[1-8] Ethylene/1-olefin copolymers made with these catalysts can be considered to be a blend of chains that follow various single-site MWDs and CCDs.

Deconvolution of microstructural characteristics is an inverse computational technique to help identify the number of site types in the catalyst and the chain microstructures produced by them. This information is very important for understanding the effect of polymerization conditions on chain microstructures made on each site type and for designing polymers with desired chain microstructures and properties.

The deconvolution of MWD obtained from gel permeation chromatography (GPC)[9-17] and CCD obtained from temperature rising elusion fractionation (TREF) or crystallization analysis fractionation (Crystaf)[18-19] has been investigated in several previous publications. However, discrepancies between the number of site types and kinetic parameters were observed when the MWD and CCD of the same sample were deconvoluted separately,[18] possibly because some site types may produce chains with similar molecular weight averages but different mean comonomer content or vice versa, suggesting that molecular weight and comonomer composition information should be considered at the same time to yield more consistent results.

The simultaneous deconvolution of molecular weight and chemical composition distributions (MWD + CCD) have been investigated in our research group to address this issue.[20-23]

Developments in hyphenated fractionation techniques for polyolefins provide a great wealth of microstructural information, leading to several alternatives for simultaneous deconvolution strategies. Examples of hyphenated techniques include GPC-IR,[24-25] which generates the molecular weight distribution and average comonomer content at each molecular weight (MWD×CC), and TREF-LS or CRYSTAF-LS,[26-29] which provides chemical composition distribution and average molecular weight at each comonomer composition (CCD×MW). These techniques are also referred to as semi cross-fractionation because the polymer is fractionated according either MWD or CCD and the averages of the other property are calculated across the distribution. Full cross-fractionation techniques by GPC/TREF or TREF/GPC can recover the complete bivariate molecular weight and chemical composition distribution (MWD×CCD), which describe the detailed interrelationship between MW and CC.[30-31]

Based on these different analytical techniques, four simultaneous deconvolution methods will be considered in the present publication: 1) MWD×CC, measured with GPC-IR, 2) MWD + CCD, analyzed separately with GPC and TREF or CRYSTAF, 3) MWD×CC + CCD, obtained from GPC-IR and TREF or CRYSTAF, and 4) MWD×CCD, measured by GPC/TREF or TREF/GPC cross fractionation.

The four deconvolution strategies were tested using a simulated ethylene/1-butene copolymer assumed to be made with a 5 site type catalyst. The number of site types, chain microstructural properties, and weight fractions of polymers produced on

each site type indentified by each method were compared with the simulation parameters used model the polymer microstructure to identify which deconvolution strategy best described the MWD and CCD of the copolymers.

Theoretical Background

Single-Site Microstructural Distributions

The weight distribution for kinetic chain length (r) and chemical composition (F_1) of copolymers made on each site type is assumed to follow Stockmayer's bivariate distribution.[32-33] Stockmayer's distribution for linear binary copolymers is expressed as follows,

$$w(r,F_1) = r \cdot \tau^2 \cdot \exp(-r \cdot \tau) \cdot \frac{1}{\sqrt{2\pi\beta/r}} \cdot \exp\left[-\frac{(F_1 - \overline{F_1})^2}{2\beta/r} \right] \quad (1)$$

$$\beta = \overline{F_1} \cdot (1 - \overline{F_1}) \cdot \sqrt{1 + 4 \cdot \overline{F_1} \cdot (1 - \overline{F_1}) \cdot (r_1 \cdot r_2 - 1)} \quad (2)$$

where τ is the ratio of the sum of all transfer rates to the propagation rate, $\overline{F_1}$ is the average mole fraction of monomer type 1 in the copolymer, and r_1 and r_2 are the copolymerization reactivity ratios. Note that the number average chain length is given by $1/\tau$. Therefore, the number average molecular weight (M_n) can be calculated as $M_n = M_{ru}/\tau$, where M_{ru} is the average molecular mass of the repeating unit in the copolymer chains.

The MWD component of Stockmayer's distribution, Flory's most probable distribution, is obtained by integrating Stockmayer's distribution over all chemical compositions,

$$w(r) = r \cdot \tau^2 \cdot \exp(-r \cdot \tau) \tag{3}$$

Similarly, the CCD component of Stockmayer's distribution is calculated by integrating Stockmayer's distribution over all chain lengths,

$$w(F_1) = \frac{3}{4\sqrt{2\beta\tau}\left[1 + \frac{(F_1 - \overline{F_1})^2}{2\beta\tau}\right]^{5/2}} \tag{4}$$

For copolymer chains produced on each site type, the average mole fractions of monomer type 1 are statistically independent of the kinetic chain length; long chains and short chains have the same average chemical composition.

Chain Microstructures for Polymers made with Multiple-Site-Type Catalysts

The microstructure of polymers produced with multiple-site-type catalysts can be modeled as a weighted average of the chain microstructures made on each site type. Therefore, the bivariate MWD×CCD can be calculated from a superposition of Stockmayer's distributions,

$$w(r, F_1) = \sum_{i=1}^{n} m_i w_i(r, F_1) \tag{5}$$

where n is the number of site types, m_i is the mass fraction of polymer made on site type i, and $w_i(r, F_1)$ is the Stockmayer's distribution of polymers made on site type i.

Similarly, the MWD and CCD of polymers synthesized with multiple-site-type catalysts is given by,

$$w(r) = \sum_{i=1}^{n} m_i w_i(r) \tag{6}$$

$$w(F_1) = \sum_{i=1}^{n} m_i w_i(F_1) \tag{7}$$

where $w_i(r)$ and $w_i(F_1)$ are the MWD and CCD of copolymers produced on site type i, respectively, as given by Equation (3) and (4).

For copolymer chains made with multiple-site-type catalysts in which each site type produces copolymer chains with different average comonomer fractions, the average mole fractions of monomer type 1 as a function of the kinetic chain length can be calculated with the following equation,

$$F_1(r) = \sum_{i=1}^{n} m_i w_i(r) \overline{F}_{1,i} \tag{8}$$

where $\overline{F}_{1,i}$ is average mole fraction of monomer type 1 produced on site type i.

Deconvolution of Microstructural Characteristics

Deconvolution Procedure

Ideally, the deconvolution of any weight distribution function (Equations (5) to (8)) should identify the same number of site types and yield the same set of mass fractions and kinetic parameters for each site type. However, independent deconvolutions of MWD and CCD were reported to lead to a different number of site types and slightly different set of mass fractions and kinetic parameters.[18] Differences in site type number are expected, as some site types may produced chains with similar average molecular weights but different comonomer contents, or vice versa. Therefore, the number of site types identified from the MWD could be different from the number estimated from the CCD. Differences in polymer mass fractions and microstructural parameters per site type is also not surprising given that analytical errors in GPC, TREF and Crystaf are not the same. Therefore, it seems logical that using both distributions, or at least one distribution and the average values for the other, would lead to more consistent parameter estimates for both MWD and CCD.

In this publication, we investigate for sets of simulated data: (1) MWD×CC, (2) MWD + CCD, (3) MWD×CC + CCD, and (4) MWD×CCD. These alternative deconvolution approaches are easily applicable actual polymers, since the required microstructural information can be obtained experimentally using available automated semi- and full cross-fractionation techniques, as discussed above.

The following procedure was used for all deconvolutions:

1) The calculations were started by assuming that the number of site types was 2. The method used to find the initial guesses for these parameters is discussed in the next section.
2) The simultaneous deconvolution was performed by matching the modeled polymer structure with the proper distributions described above.

3) The objective functions (the sum of the squares of differences between microstructural distributions and model predictions) were given be by following equations,

Strategy 1: Deconvolution of MWD×CC (GPC-IR)

$$\sigma^2_{MWD\times CC} = \frac{1}{N_r}\sum_r [w_{\exp}(r) - w_{sim}(r)]^2 + \frac{1}{N_r}\sum_r [F_{1,\exp}(r) - F_{1,sim}(r)]^2 \qquad (9)$$

Strategy 2: Deconvolution of MWD + CCD (GPC + TREF)

$$\sigma^2_{MWD+CCD} = \frac{1}{N_r}\sum_r [w_{\exp}(r) - w_{sim}(r)]^2 + \frac{1}{N_F}\sum_{F_1} [w_{\exp}(F_1) - w_{sim}(F_1)]^2 \quad (10)$$

Strategy 3: Deconvolution of MWD×CC + CCD (GPC-IR + TREF)

$$\begin{aligned}\sigma^2_{MWD\times CC+CCD} = & \frac{1}{N_r}\sum_r [w_{\exp}(r) - w_{sim}(r)]^2 \\ & + \frac{1}{N_F}\sum_{F_1} [w_{\exp}(F_1) - w_{sim}(F_1)]^2 \\ & + \frac{1}{N_r}\sum_r [F_{1,\exp}(r) - F_{1,sim}(r)]^2\end{aligned} \qquad (11)$$

Strategy 4: Deconvolution of MWD×CCD (Cross Fractionation)

$$\sigma^2_{MWD\times CCD} = \frac{1}{N_{r\times F}}\sum_{F_i}\sum_r [w_{\exp}(r, F_1) - w_{sim}(r, F_1)]^2 \qquad (12)$$

where N_r, N_F, and $N_{r\times F}$ are the number of data points for MWD, CCD, and MWD×CCD cross-fractionation, respectively, and $w_{sim}(r, F_1)$, $w_{sim}(r)$, $w_{sim}(F_1)$, and $F_1(r)$ can be calculated with Equation (5) to (8).

4) The kinetic parameters and mass fraction of polymer made on each site type were estimated and the value of the objective function was recorded. For *n* site types, 4*n*-1 parameters must be estimated because there are 4 parameters per site type (*m*, $\overline{F_1}$, β, and τ) and one constraint equation ($\sum_{i=1}^{n} m_i = 1$).

5) The number of site types was then gradually increased and the calculation repeated until the value of the objective function stopped decreasing or did not decrease significantly with an increase in the number of site types.

Obtaining Initial Guesses for the Deconvolution Parameters

Initial guesses for the model parameters (*m*, $\overline{F_1}$, β, and τ) were obtained using the following procedure. For parameters *m* and τ, initial guesses for 2 catalyst site types were estimated from the knowledge of the number, weight, and z average molecular weights, which can be calculated from the experimental MWD, by solving the following equations,[9]

$$\frac{M_n}{M_{ru}} = \frac{1}{m_1\tau_1 + m_2\tau_2} \tag{13}$$

$$\frac{M_w}{M_{ru}} = 2\left(\frac{m_1}{\tau_1} + \frac{m_2}{\tau_2}\right) \tag{14}$$

$$\frac{M_z}{M_{ru}} = 3\left(\frac{m_1}{\tau_1^{\,2}} + \frac{m_2}{\tau_2^{\,2}}\right)\left(\frac{m_1}{\tau_1} + \frac{m_2}{\tau_2}\right)^{-1} \tag{15}$$

where M_{ru} is the average molecular weight of the repeating unit. Note that for the case of two site types, $m_1 + m_2 = 1$.

The initial guesses for m and τ in the case of $n + 1$ ($n > 2$) site types was estimated from the converged values for the parameters m and τ for the previous iteration with n site types. The parameter τ for site n+1 (τ_{n+1}) was estimated as the weight average of parameter τ for n site types ($\tau_{n+1} = \sum_{i=1}^{n} m_i \tau_i$). The parameter m for site type n+1 (m_{n+1}) was first assumed to be the average of the m_i values for the adjacent sites to τ_{n+1}, and then the new set of parameters m was normalized so that $\sum_{i=1}^{n+1} m_i = 1$.

Considering that the initial guesses for parameter $\overline{F_1}$ of each site type was evenly distributed within the experimental range of $\overline{F_1}$, the value of parameter $\overline{F_1}$ for site type i ($\overline{F_{1,i}}$) was estimated by

$$\overline{F_{1,i}} = \overline{F_{1,\min}} + i\frac{(\overline{F_{1,\max}} - \overline{F_{1,\min}})}{(n+1)} \tag{16}$$

where $\overline{F_{1,\max}}$ and $\overline{F_{1,\min}}$ are the maximum and minimum values of the experimental range of $\overline{F_1}$ and n is the total number of site types.

The initial guess for parameter β for site type i (β_i) was estimated by assuming that the copolymer is a perfect random copolymer ($r_1 r_2 = 1$).

$$\beta_i = \overline{F_{1,i}}(1 - \overline{F_{1,i}}) \tag{17}$$

The above guess estimation process was found to be very useful in helping to achieve the minimization of objective functions described in Equation (9) – (12).

Model Copolymers for Comparison of Four Simultaneous Deconvolution Approaches

In order to compare the four simultaneous deconvolution strategies outlined above, the microstructure of an ethylene/1-butene copolymer was simulated assuming a catalyst with five site types. The model parameters are summarized in Table 1. In this study, F_1 represents the mole fraction of ethylene in the copolymer. Figures 1 shows the simulated chain microstructure for this copolymer.

Results and Discussion

Deconvolution of MWD×CC (GPC-IR)

The MWD and the relation between MW and CC obtained from the deconvolution of MWD×CC information are shown in Figure 2 and 3. Table 2 shows mass fraction and kinetic parameters for each site type. The value of the objective function $\sigma^2_{MWD\times CC}$ varies with the number of site types as shown in Table 3.

The deconvolution procedure was able to identify 5 site types as the best model fit, leading to the minimum value of objective function $\sigma^2_{MWD\times CC}$. A smaller number of site types cannot adequately describe the MWD (Figure 2), albeit a reasonable fit of the relationship between MW and CC is already obtained with 3 site

types (Figure 2). When the number of site type increases from 2 to 5, the objective function decreases, but increasing the number of sites to 6 makes it to also increase, indicating that five site types is a more adequate fit to the experimental data (Table 3).

The values estimated for the model parameters are close to those used to generate the model copolymer microstructure, with less than ±1% deviation, except the parameter β with up to more than ±500% error. This is not surprising because parameter β is not directly present in the model equation describing MWD×CC. In fact, this parameter is strongly related to the broadness of CCD, the information that was not considered in this deconvolution strategy. Therefore, the parameter β was very roughly calculated from the guess estimation process as described in the previous section.

This error can be clearly seen when CCDs obtained from deconvolution are compared with model CCDs as shown in Figure 4. Therefore, although the deconvolution of MWD×CC information can accurately identify the number of active site type, MWD, and the relationship between MW and CC, it is simply insufficient for describing the CCD.

Deconvolution of MWD + CCD (GPC + TREF)

The relation between MW and CC is insufficient to estimate the parameter β, the CCD needs to be considered in the deconvolution procedure if one wants to also predict the CCD. Figure 5 and 6 show MWD and CCD obtained from the simultaneous deconvolution of MWD + CCD, and Table 4 shows the values estimated for the model parameters of each site type. The objective function $\sigma^2_{MWD+CCD}$ varies with the number of site types as shown in Table 5.

Similarly to the previous case, 5 site types are identified as the best fit for the polymer microstructure. When a smaller number of site types is considered, MWD and CCD of the model copolymer cannot be adequately described. The minimum value for $\sigma^2_{MWD+CCD}$ was also found when 5 site types where considered.

As the relationship between MW and CC was not considered in this deconvolution strategies, the results of such relationship obtained from parameters estimated from this deconvolution strategies clearly deviated from the model copolymers when an inadequate number of site types was considered (see Figure 7). However, for 5 site types, the relationship between MW and CC was properly predicted.

All estimated mass fraction and kinetic parameters of each site type obtained from this deconvolution strategy were found to be close to those of the model copolymer with less than ±3% error.

Deconvolution of MWD×CC + CCD (GPC/IR + TREF)

Another alternative strategy for simultaneous microstructural deconvolution is to combine the MWD×CC information available from GPC-IR semi-cross fractionation with CCD that could be obtained from TREF or CRYSTAF to help enhance the parameter estimation process.

Figure 8, 9, and 10 show the MWD, the relation between MW and CC, and the CCD obtained from the deconvolution of MWD×CC + CCD, and Table 6 summarizes the model parameter estimates. The objective function $\sigma^2_{MWD\times CC+CCD}$ depends on the number of site types as shown in Table 7.

As expected, this deconvolution strategy also predicted that five site types gives the best fit and led to the minimum value of objective function $\sigma^2_{MWD\times CC+CCD}$. Because the relationship between MW and CC was also taken into account in the objective function, the relationship between MW and CC obtained from the deconvolution was found to converge to that of model copolymers faster than the previous case when it was absent (compare Figure 7 and 9).

However, the final parameter estimates are not significantly better than for the second case study. All model parameters obtained from this deconvolution strategy were found to have about the same deviation from those used to simulate the copolymer microstructure (< ±3%).

Deconvolution of MWD×CCD (Cross-Fractionation)

The last simultaneous deconvolution strategy used the complete bivariate MWD×CCD, an information that can be obtained from automated GPC/TREF or TREF/GPC cross fractionation. This joint distribution provides the detailed interrelationship between MW and CC, thus giving the most comprehensive microstructural distribution for ethylene/1-olefin copolymers.

Figure 11 shows the contour plots for the bivariate MWD× CCD obtained from deconvolution, while Table 8 lists the parameter estimates for each site type. The values of the objective function $\sigma^2_{MWD\times CCD}$ vary with the number of site types as shown in Table 9.

Besides being able to accurately identify the number of site types, this simultaneous deconvolution strategy provided the most accurate parameter estimates, with maximum error values of less than 1.0×10^{-6}.

Comparison of Deconvolution Strategies

All simultaneous deconvolution strategies investigated can correctly identify the number of site types and estimate the model parameters for each site type. However, the simultaneous deconvolution of MWD×CC cannot estimate the parameter β nor describe CCD of the model ethylene/1-butene copolymer.

Simultaneous deconvolutions of MWD + CCD and MWD×CC + CCD provide practically the same final results. Due to the most comprehensive microstructural information, the simultaneous deconvolution of MWD×CCD information provides the most accurate model estimation. Table 10 compares the results obtained from different simultaneous deconvolution strategies based on the objective function $\sigma^2_{MWD\times CCD}$. In all cases, the results from deconvolution of MWD×CCD information was found to be superior to the other strategies with significantly less value of the objective function $\sigma^2_{MWD\times CCD}$.

It is important to note, however, that the actual numerical magnitudes of differences in estimated parameters of these last three strategies are, in fact, rather minimal (see Table 4, 6, and 8) and the experimental error of the results used for deconvolution could have a greater impact. In practice, peak broadening and cocrystallization during the characterization process could significantly affect the accuracy of MWD and CCD information and the quality of the simultaneous deconvolution results. This issue is currently under investigation in our laboratory and will be the subject of future publication.

Conclusions

To identify the number of site types and estimate mass fraction and kinetic parameters of each active site type for ethylene/1-olefin copolymers synthesized with multiple-site-type catalytic systems, the simultaneous deconvolution strategies of MWD and CCD were studied. Four simultaneous deconvolution strategies based on (1) MWD×CC, (2) MWD + CCD, (3) MWD×CC + CCD, and (4) MWD×CCD information were validated with the model ethylene/1-butene copolymers and compared. All strategies can accurately identify the number of site types. However, the first strategy based on MWD×CC information cannot adequately estimate parameter β and describe CCD. The simultaneous deconvolutions of MWD + CCD and MWD×CC + CCD give equivalent results. The last strategy using MWD×CCD information was found to provide the most accurate estimation of mass fraction and kinetic parameters of each site type theoretically.

Acknowledgements

Siripon Anantawaraskul thanks The Thailand Research Fund (TRF), Kasetsart University Research and Development Institute (KURDI), and Center of Excellence for Petroleum, Petrochemicals and Advanced Materials of Thailand (PPAM) for their kind financial support.

References

[1] J. B. P. Soares, J. D. Kim, G. L. Rempel, *Ind. Eng. Chem. Res.* **1997**, *36*, 1144.

[2] J. Huang, G. L. Rempel, *Prog. Polym. Sci*. **1995**, *20*, 459.

[3] S. S. Reddy, S. Sivaram, *Prog. Polym. Sci*. **1995**, *20*, 309.

[4] A. E. Hamielec, J. B. P. Soares, *Prog. Polym. Sci*. **1996**, *21*, 651.

[5] J. B. P. Soares, J. D. Kim, *J. Polym. Sci. Part A: Polym. Chem.* **2000**, *38*, 1408.

[6] J. D. Kim, J. B. P. Soares, *J. Polym. Sci. Part A: Polym. Chem.* **2000**, *38*, 1417.

[7] J. D. Kim, J. B. P. Soares, *J. Polym. Sci. Part A: Polym. Chem.* **2000**, *38*, 1427.

[8] K. Narkchamnan, S. Anantawaraskul, J. B.P. Soares, *Macromol. React. Eng*. DOI = 10.1002/mren.201100002

[9] J. B. P. Soares, A. E. Hamielec, *Polymer* **1995**, *36*, 2257.

[10] Y. V. Kissin, *J. Polym. Sci. Part A: Polym. Chem*. **1995**, *33*, 227.

[11] J. B. P.Soares, *Polym. React. Eng*. **1998**, *6*, 225.

[12] J. B. P. Soares, R. F. Abbott, J. N. Willis, X. Liu, *Macromol. Chem. Phys*. **1996**, *197*, 3383.

[13] Y. V. Kissin, R. I. Mink, T. E. Nowlin, *J. Polym. Sci. Part A: Polym. Chem.* **1999**, *37*, 4255.

[14] Y. V. Kissin, *J. Polym. Sci. Part A: Polym. Chem*. **2001**, *39*, 1681.

[15] D. E. Thompson, K. B. McAuley, P. J. McLellan, *Macromol. React. Eng*. **2007**, *1*, 523.

[16] D.E. Thompson, K. B. McAuley, P. J. McLellan, *Macromol. React. Eng.* **2007**, *1*, 264.

[17] M. A. Matsko, L. G. Echevskaya, V. A. Zakharov, M. I. Nikolaeva, T. B. Mikenas, M. P. Vanina, *Macromol. Symp.* **2009**, *282*, 157.

[18] A. A. Da Silva Filho, J. B. P.Soares, G. B. de Galland , *Macromol. Chem. Phys.* **2000**, *201*, 1226.

[19] A. Faldi, J. B. P. Soares, *Polymer* **2001**, *42*, 3057.

[20] A. A. Alghyamah, J. B. P. Soares, *Macromol. Rapid Commun.* **2009**, *30*, 384.

[21] A. A. Alghyamah, J. B. P. Soares, *Macromol. Symp.* **2009**, *285*, 81.

[22] S. Anantawaraskul, W. Bongsontia, J. B.P. Soares, *Macromol. Symp.* **2009**, *282*, 167.

[23] M. A. Al-Saleh, J. B. P. Soares, T. A. Duever, *Macromol. React. Eng.* **2010**, *4*, 578.

[24] A. Ortín, B. Monrabal, J. Montesinos, P. del Hierro, *Macromol. Symp.* **2009**, *282*, 65.

[25] I. Suárez, M. J. Caballero, B. Coto, *Polym. Eng. Sci*. **2011**, *51*, 317.

[26] L. Wild, *Adv. Polym. Sci.* **1990**, *98*, 1.

[27] B. Monrabal, *J. Appl. Polym. Sci.* **1994**, *52*, 491.

[28] S. Anantawaraskul, J. B. P. Soares, P. M. Wood-Adams, *Adv. Polym. Sci.* **2005**, *182*, 1.

[29] J. B. P. Soares, S. Anantawaraskul, *J. Polym. Sci. Part B: Polym. Phys.* **2005**, *43*, 1557.

[30] A. Ortin, B. Monrabal, J. Sancho-Tello, *Macromol. Symp*. **2007**, *257*, 13.

[31] W. W. Yau, *Macromol. Symp*. **2007**, *257*, 29.

[32] W. H. Stockmayer, *J. Chem. Phys.* **1945**, *13*, 199.

[33] R. Simha, H. Branson, *J. Chem. Phys*. **1944**, *12*, 253.

Table Captions

Table 1. Model parameters for the model ethylene/1-butene copolymer.

Table 2. Summary of estimated mass fraction and kinetic parameters of each site type obtained from the simultaneous deconvolution of MWD×CC information.

Table 3. Value of the objective function $\sigma^2_{MWD\times CC}$ as a function of the number of site types.

Table 4. Summary of estimated mass fraction and kinetic parameters of each site type obtained from the simultaneous deconvolution of MWD + CCD information.

Table 5. Value of the objective function $\sigma^2_{MWD+CCD}$ as a function of the number of site types.

Table 6. Summary of estimated mass fraction and kinetic parameters of each site type obtained from the simultaneous deconvolution of MWD×CC + CCD information.

Table 7. Value of the objective function $\sigma^2_{MWD\times CC+CCD}$ as a function of the number of site types.

Table 8. Summary of estimated mass fraction and kinetic parameters of each site type obtained from the simultaneous deconvolution of MWD×CCD information.

Table 9. Value of the objective function $\sigma^2_{MWD\times CCD}$ as a function of the number of site types.

Table 10. Comparison of objective function $\sigma^2_{MWD\times CCD}$ obtained from different simultaneous deconvolution strategies.

Figure Captions

Figure 1. Chain microstructures of the model ethylene/1-butene copolymer: (a) MWD, (b) CCD, (c) MW/CC relationship, and (d) MWD/CCD contour plot.

Figure 2. MWD obtained from deconvolution of MWD×CC information of the model ethylene/1-butene copolymer using a different number of site types: (a) 2, (b) 3, (c) 4, and (d) 5. Symbol (□) is the simulation data, solid line indicates the deconvolution results from all site types, and dot line indicates contribution from each site type.

Figure 3. Relationship between MW and CC obtained from deconvolution of MWD×CC information of the model ethylene/1-butene copolymer using a different number of site types: (a) 2, (b) 3, (c) 4, and (d) 5. Symbol (□) is the simulation data. Solid line indicates the deconvolution results from all site types.

Figure 4. CCD obtained from deconvolution of MWD×CC information of the model ethylene/1-butene copolymer using a different number of site types: (a) 2, (b) 3, (c) 4, and (d) 5. Symbol (□) is the simulation data, solid line indicates the deconvolution results from all site types, and dot line indicates contribution from each site type

Figure 5. MWD obtained from deconvolution of MWD + CCD information of the model ethylene/1-butene copolymer using a different number of site types: (a) 2, (b) 3, (c) 4, and (d) 5. Symbol (□) is the simulation data, solid line indicates the deconvolution results from all site types, and dot line indicates contribution from each site type.

Figure 6. CCD obtained from deconvolution of MWD + CCD information of the model ethylene/1-butene copolymer using a different number of site types: (a) 2, (b) 3, (c) 4, and (d) 5. Symbol (□) is the simulation data, solid line indicates the deconvolution results from all site types, and dot line indicates contribution from each site type

Figure 7. The relationship between MW and CC obtained from deconvolution of MWD + CCD information of the model ethylene/1-butene copolymer using a different number of site types: (a) 2, (b) 3, (c) 4, and (d) 5. Symbol (□) is the simulation data. Solid line indicates the deconvolution results from all site types.

Figure 8. MWD obtained from deconvolution of MWD×CC + CCD information of the model ethylene/1-butene copolymer using a different number of site types: (a) 2, (b) 3, (c) 4, and (d) 5. Symbol (□) is the simulation data, solid line indicates the deconvolution results from all site types, and dot line indicates contribution from each site type.

Figure 9. Relationship between MW and CC obtained from deconvolution of MWD×CC + CCD information of the model ethylene/1-butene copolymer using a different number of site types: (a) 2, (b) 3, (c) 4, and (d) 5. Symbol (□) is the simulation data. Solid line indicates the deconvolution results from all site types.

Figure 10. CCD obtained from deconvolution of MWD×CC + CCD information of the model ethylene/1-butene copolymer using a different number of site types: (a) 2,

(b) 3, (c) 4, and (d) 5. Symbol (□) is the simulation data, solid line indicates the deconvolution results from all site types, and dot line indicates contribution from each site type.

Figure 11. MWD×CCD contour plot obtained from deconvolution of MWD×CCD information of the model ethylene/1-butene copolymer using a different number of site types: (a) 2, (b) 3, (c) 4, and (d) 5.

Table Captions (for Supplementary Documents)

Table S1. Summary of estimated mass fraction and kinetic parameters of each site type obtained from the simultaneous deconvolution of MWD×CC information using a different number of site types: (a) 2, (b) 3, (c) 4, and (d) 5.

Table S2. Summary of estimated mass fraction and kinetic parameters of each site type obtained from the simultaneous deconvolution of MWD + CCD information using a different number of site types: (a) 2, (b) 3, (c) 4, and (d) 5.

Table S3. Summary of estimated mass fraction and kinetic parameters of each site type obtained from the simultaneous deconvolution of MWD×CC +CCD information using a different number of site types: (a) 2, (b) 3, (c) 4, and (d) 5.

Table S4. Summary of estimated mass fraction and kinetic parameters of each site type obtained from the simultaneous deconvolution of MWD×CCD information using a different number of site types: (a) 2, (b) 3, (c) 4, and (d) 5.

Table 1. Model parameters for the model ethylene/1-butene copolymer.

Model parameters	Active site type				
	1	2	3	4	5
m	0.0160	0.2300	0.4000	0.2000	0.1540
$\overline{F_1}$	0.8838	0.9208	0.9500	0.9795	0.9841
β	0.0087	0.1427	0.3461	0.1177	0.1397
M_n	3,960	12,700	32,000	72,800	181,000

Table 2. Summary of estimated mass fraction and kinetic parameters of each site type obtained from the simultaneous deconvolution of MWD×CC information.

Parameters	Site type				
	1	2	3	4	5
m	0.0161	0.2293	0.4006	0.2000	0.1540
(% error)	(0.582)	(-0.294)	(0.151)	(0.007)	(-0.023)
$\overline{F_1}$	0.8848	0.9207	0.9500	0.9795	0.9841
(% error)	(0.110)	(-0.014)	(-7.31E-05)	(-0.001)	(2.45E-05)
β	0.0900	0.0736	0.0564	0.0384	0.0196
(% error)	(515.328)	(-71.031)	(-91.225)	(-83.185)	(-92.817)
M_n	3,931	12,683	31,972	72,803	181,003
(% error)	(-0.723)	(-0.138)	(-0.089)	(0.004)	(0.002)

Table 3. Value of the objective function $\sigma^2_{MWD\times CC}$ as a function of the number of site types.

Number of site types	Objective function $\sigma^2_{MWD\times CC}$
2	2.93E-02
3	2.72E-03
4	7.53E-04
5	2.10E-08
6	1.57E-03

Table 4. Summary of estimated mass fraction and kinetic parameters of each site type obtained from the simultaneous deconvolution of MWD + CCD information.

Parameters	Site type				
	1	2	3	4	5
m	0.0158	0.2297	0.4003	0.2002	0.1539
(% error)	(-0.943)	(-0.130)	(0.068)	(0.122)	(-0.042)
$\overline{F_1}$	0.8838	0.9208	0.9500	0.9795	0.9841
(% error)	(-0.002)	(-0.004)	(-0.002)	(1.71E-04)	(-3.27E-04)
β	0.0143	0.2537	0.6423	0.2289	0.2728
(% error)	(-2.272)	(-0.137)	(-0.070)	(0.238)	(-0.022)
M_n	3,931	12,683	31,972	72,803	181,003
(% error)	(-0.722)	(-0.138)	(-0.089)	(0.004)	(0.002)

Table 5. Value of the objective function $\sigma^2_{MWD+CCD}$ as a function of the number of site types.

Number of site types	Objective function $\sigma^2_{MWD+CCD}$
2	1.82E-03
3	8.62E-05
4	1.60E-05
5	3.76E-07
6	6.46E-04

Table 6. Summary of estimated mass fraction and kinetic parameters of each site type obtained from the simultaneous deconvolution of MWD×CC + CCD information.

Parameters	Site type				
	1	2	3	4	5
m	0.0159	0.2296	0.4004	0.2002	0.1539
(% error)	(-0.795)	(-0.188)	(0.110)	(0.100)	(-0.053)
$\overline{F_1}$	0.8841	0.9207	0.9500	0.9795	0.9841
(% error)	(0.030)	(-0.011)	(-0.001)	(-0.001)	(2.41E-05)
β	0.0142	0.2530	0.6401	0.2287	0.2724
(% error)	(-2.690)	(-0.435)	(-0.412)	(0.135)	(-0.169)
M_n	3,932	12,682	31,972	72,803	181,003
(% error)	(-0.704)	(-0.141)	(-0.088)	(0.004)	(0.002)

Table 7. Value of the objective function $\sigma^2_{MWD\times CC+CCD}$ as a function of the number of site types.

Number of site types	Objective function $\sigma^2_{MWD\times CC+CCD}$
2	3.55E-02
3	2.89E-03
4	8.41E-04
5	6.83E-07
6	1.74E-03

Table 8. Summary of estimated mass fraction and kinetic parameters of each site type obtained from the simultaneous deconvolution of MWD×CCD information.

Parameters	Site type				
	1	2	3	4	5
m	0.0160	0.2300	0.4000	0.2000	0.1540
(% error)	(9.48E-08)	(2.14E-08)	(-7.75E-08)	(-1.37E-07)	(3.37E-07)
$\overline{F_1}$	0.8838	0.9208	0.9500	0.9795	0.9841
(% error)	(3.29E-09)	(-1.40E-09)	(-1.44E-09)	(-1.49E-09)	(-6.67E-10)
β	0.0146	0.2541	0.6428	0.2284	0.2729
(% error)	(4.23E-07)	(4.31E-08)	(-1.93E-07)	(4.41E-08)	(1.56E-08)
M_n	3,960	12,700	32,000	72,800	181,000
(% error)	(-1.17E-07)	(1.23E-08)	(-2.30E-09)	(-2.16E-07)	(-1.72E-07)

Table 9. Value of the objective function $\sigma^2_{MWD\times CCD}$ as a function of the number of site types.

Number of site types	Objective function $\sigma^2_{MWD\times CCD}$
2	7.63E-01
3	2.23E-01
4	7.64E-03
5	2.91E-18
6	3.72E-06

Table 10. Comparison of objective function $\sigma^2_{MWD\times CCD}$ obtained from different simultaneous deconvolution strategies.

Number of site type	Objective function $\sigma^2_{MWD\times CCD}$			
	MWD×CC	MWD + CCD	MWD×CC +CCD	MWD×CCD
2	6.73E+01	1.41E+01	6.94E+00	7.63E-01
3	1.92E+01	3.37E-01	6.14E-01	2.23E-01
4	1.16E+01	2.41E+00	5.25E-01	7.64E-03
5	8.68E+00	5.17E-06	2.22E-05	2.91E-18
6	1.55E+01	2.69E+00	1.33E+00	3.72E-06

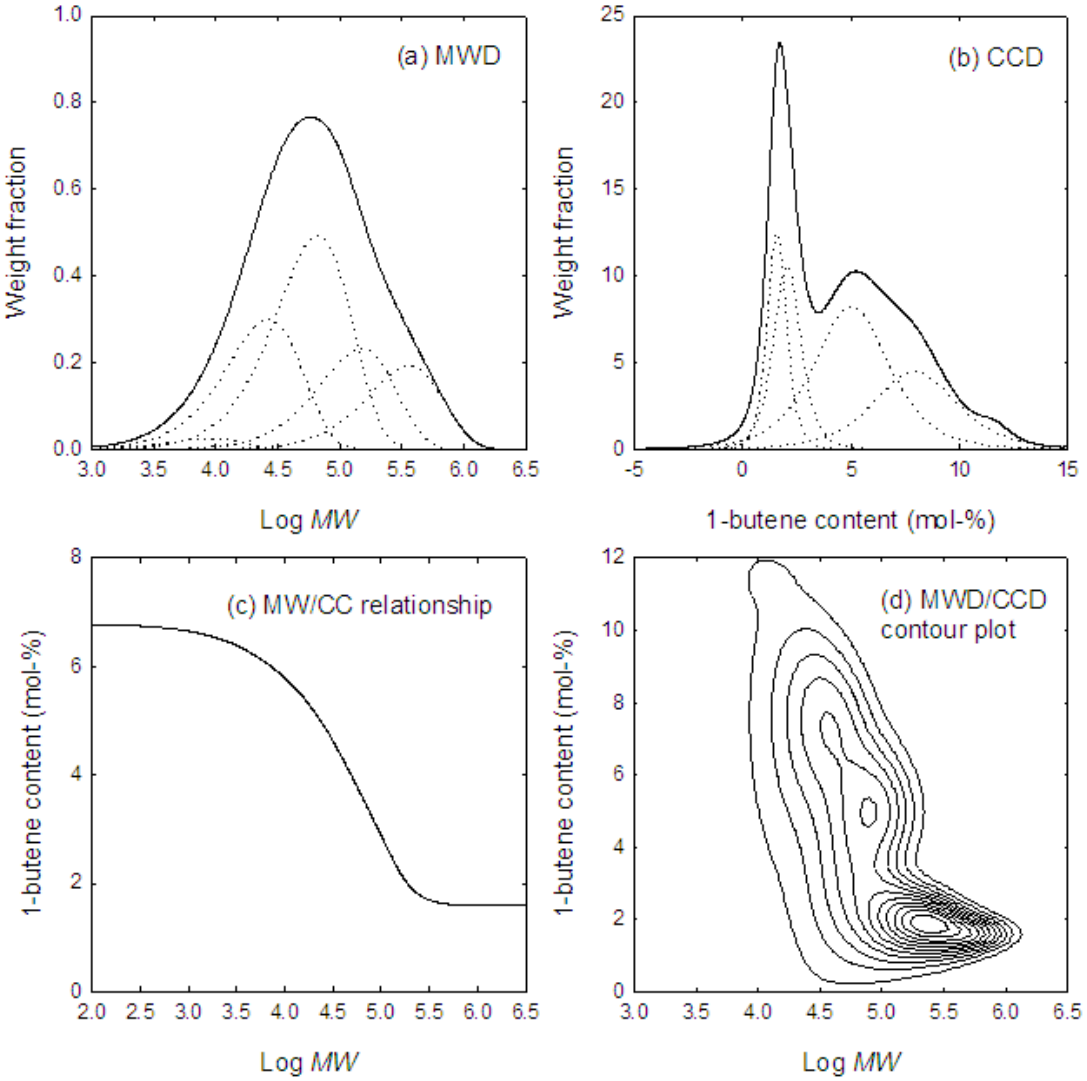

Figure 1. Chain microstructures of the model ethylene/1-butene copolymer: (a) MWD, (b) CCD, (c) MW/CC relationship, and (d) MWD/CCD contour plot.

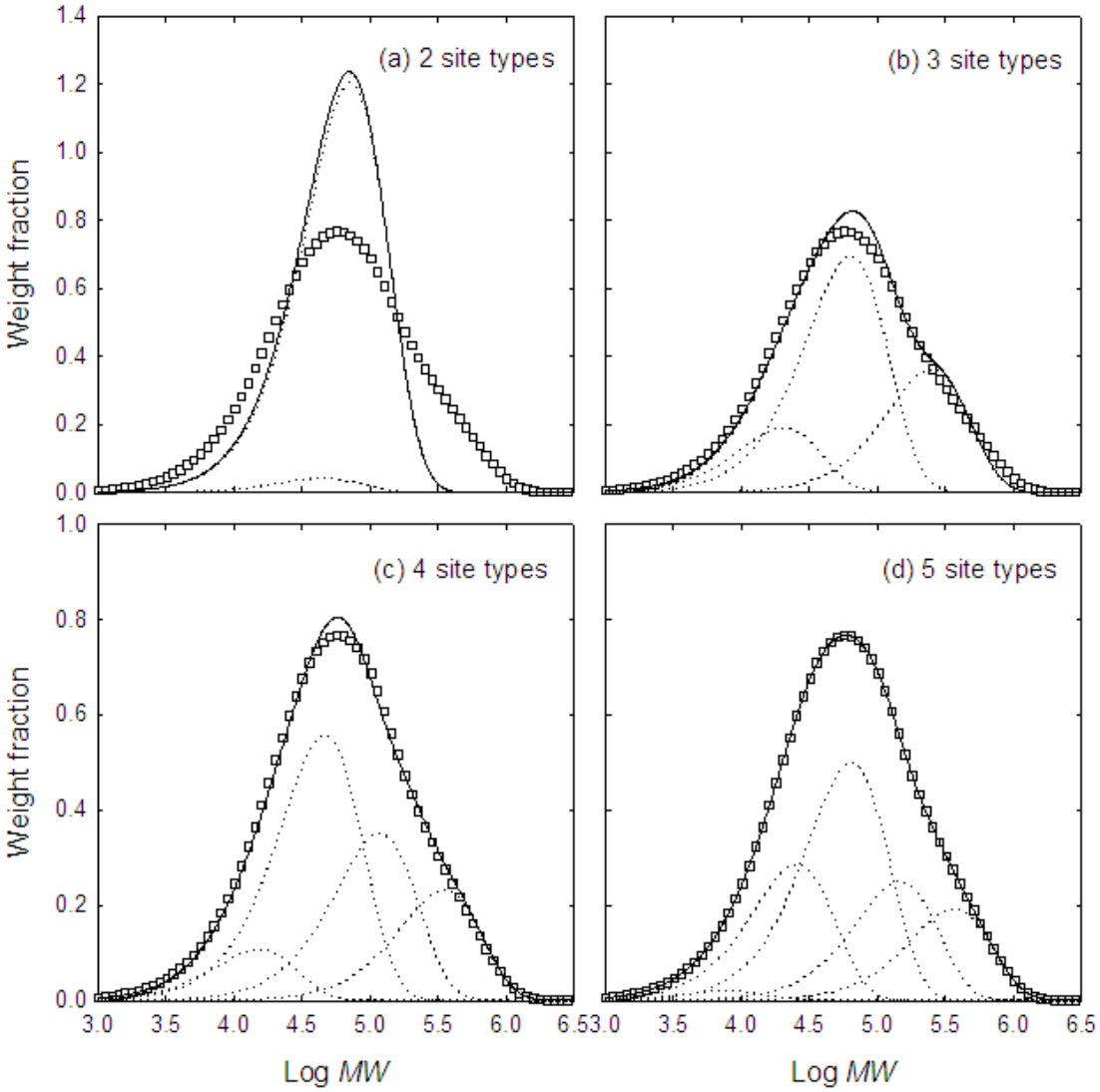

Figure 2. MWD obtained from deconvolution of MWD×CC information of the model ethylene/1-butene copolymer using a different number of site types: (a) 2, (b) 3, (c) 4, and (d) 5. Symbol (□) is the simulation data, solid line indicates the deconvolution results from all site types, and dot line indicates contribution from each site type.

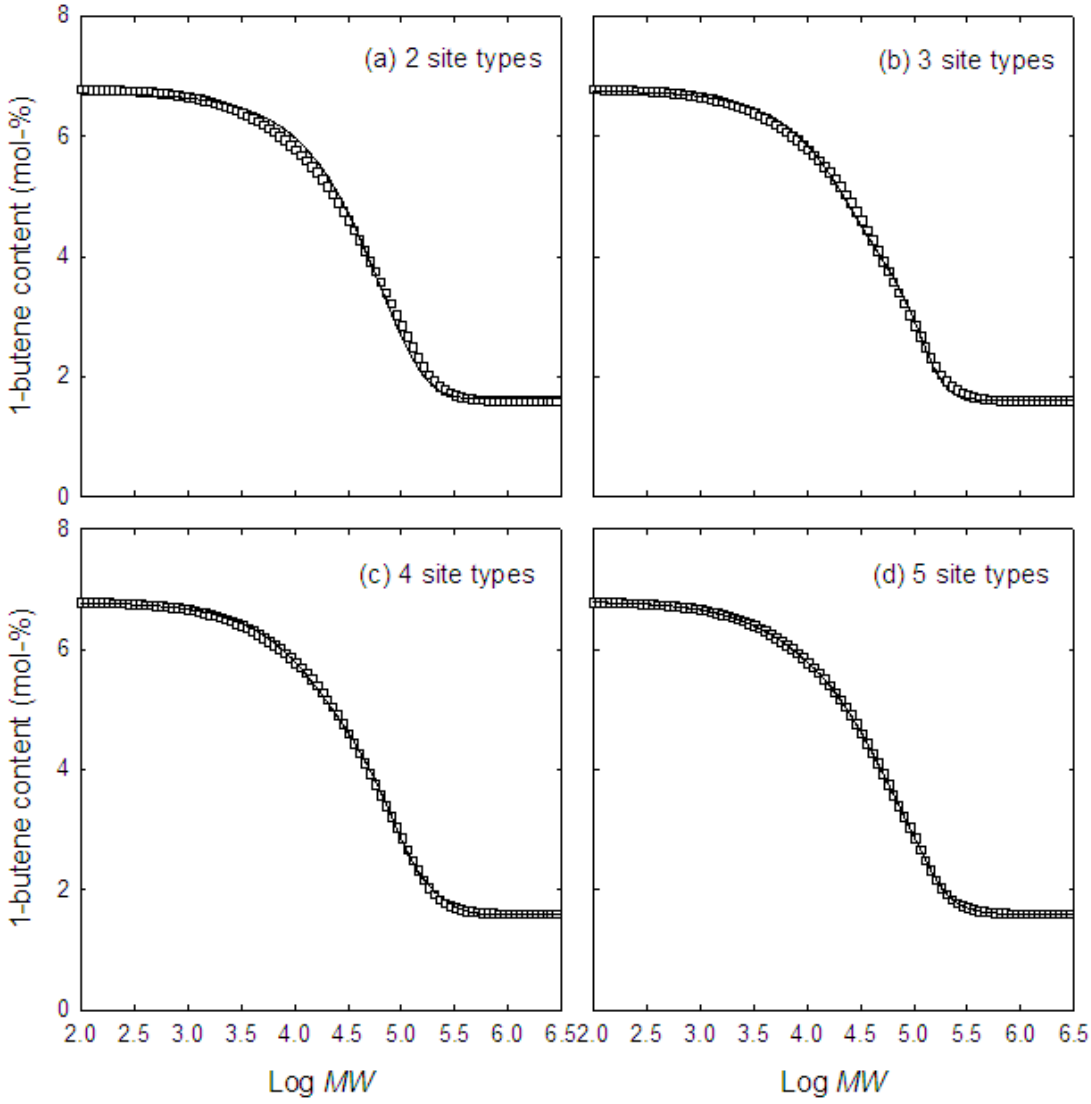

Figure 3. Relationship between MW and CC obtained from deconvolution of MWD×CC information of the model ethylene/1-butene copolymer using a different number of site types: (a) 2, (b) 3, (c) 4, and (d) 5. Symbol (□) is the simulation data. Solid line indicates the deconvolution results from all site types.

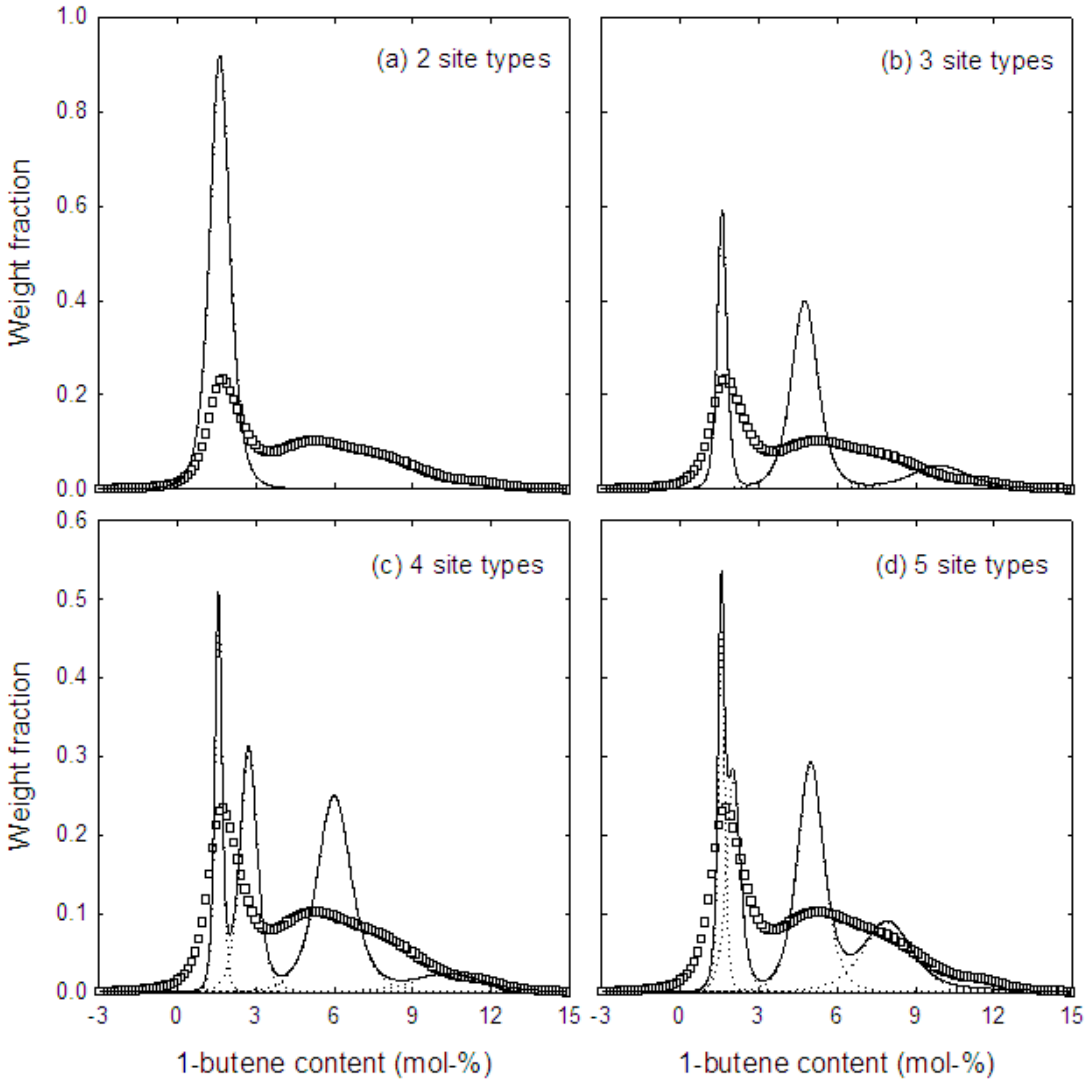

Figure 4. CCD obtained from deconvolution of MWD×CC information of the model ethylene/1-butene copolymer using a different number of site types: (a) 2, (b) 3, (c) 4, and (d) 5. Symbol (□) is the simulation data, solid line indicates the deconvolution results from all site types, and dot line indicates contribution from each site type.

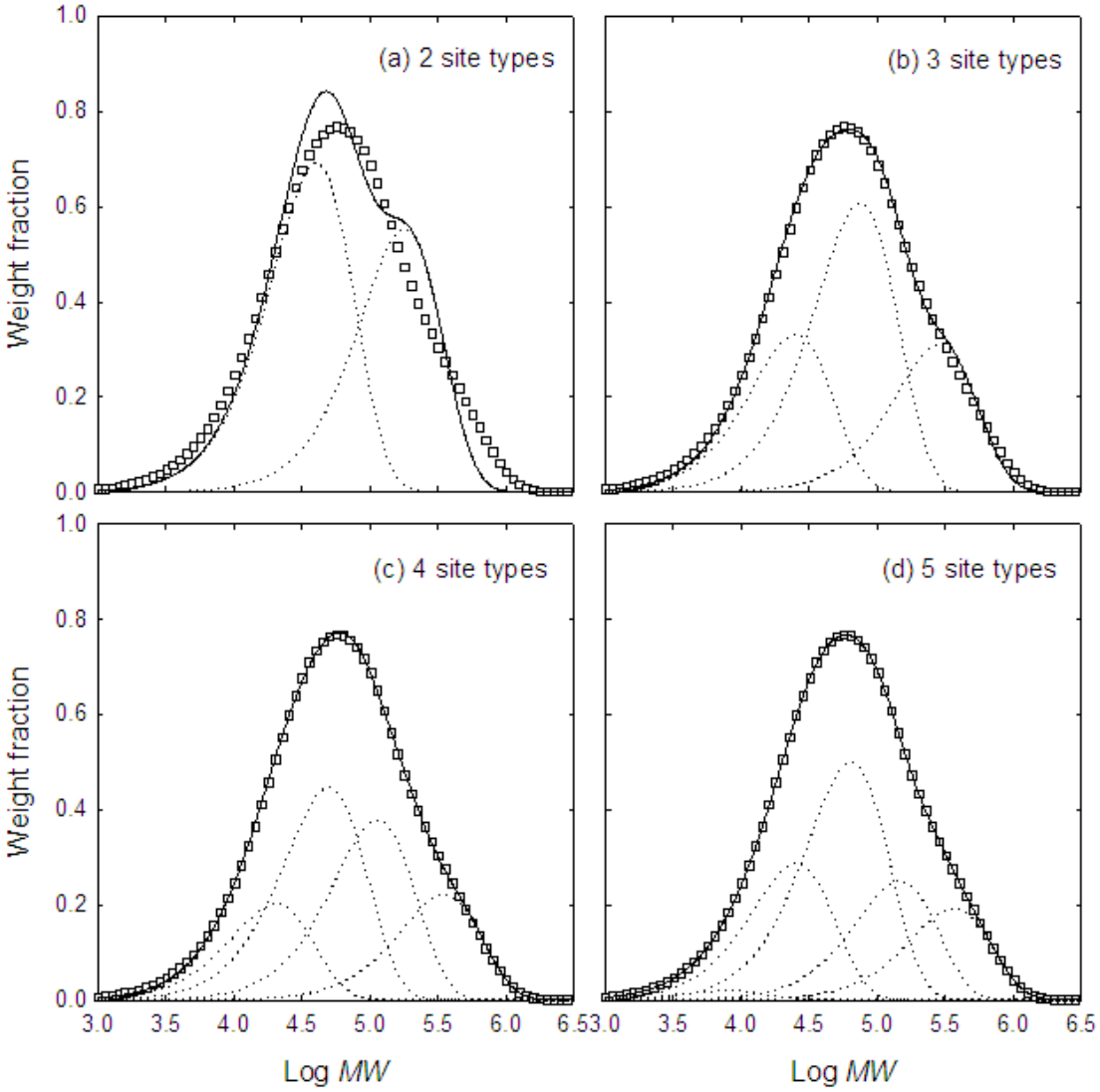

Figure 5. MWD obtained from deconvolution of MWD + CCD information of the model ethylene/1-butene copolymer using a different number of site types: (a) 2, (b) 3, (c) 4, and (d) 5. Symbol (□) is the simulation data, solid line indicates the deconvolution results from all site types, and dot line indicates contribution from each site type.

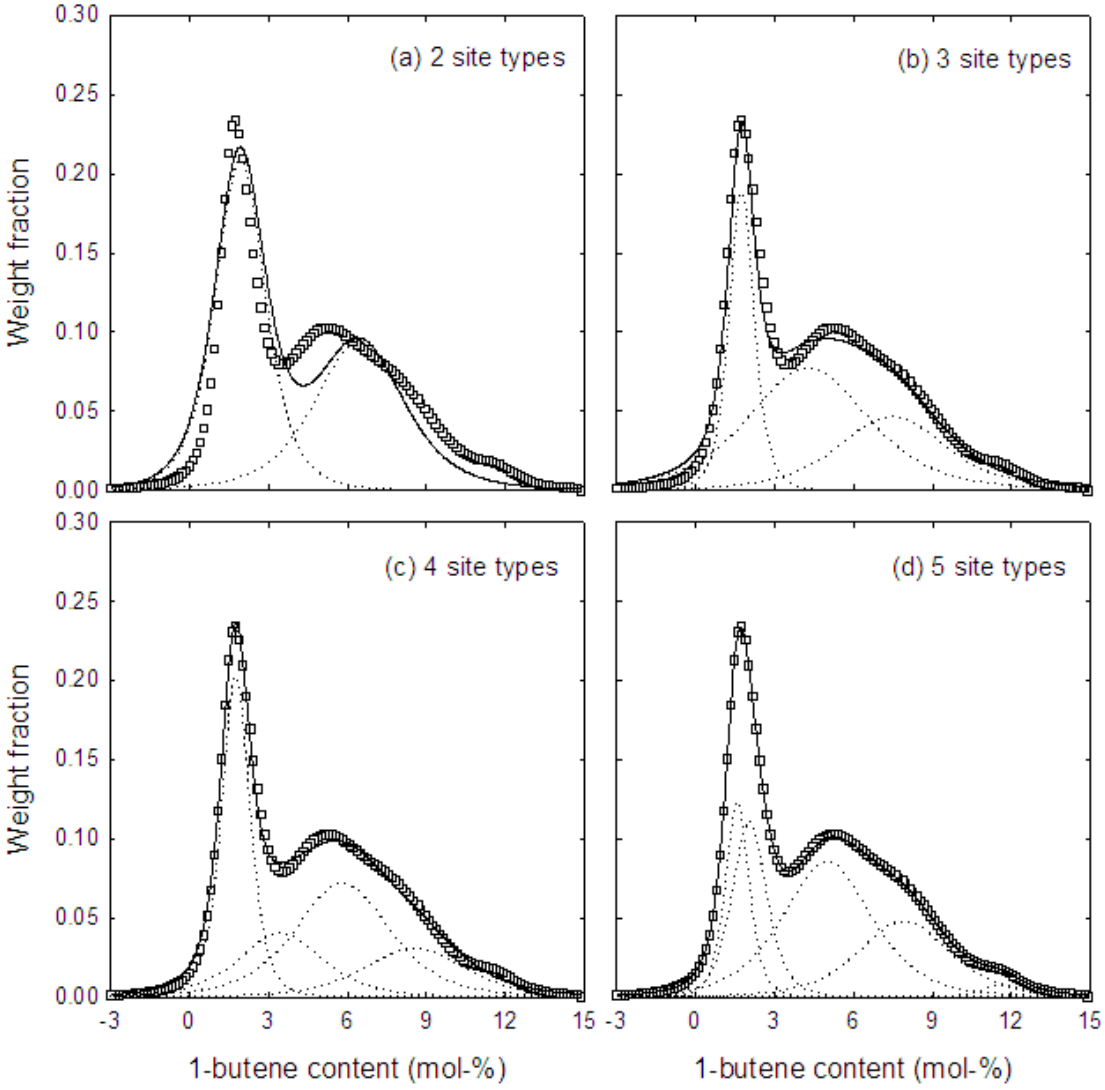

Figure 6. CCD obtained from deconvolution of MWD + CCD information of the model ethylene/1-butene copolymer using a different number of site types: (a) 2, (b) 3, (c) 4, and (d) 5. Symbol (□) is the simulation data, solid line indicates the deconvolution results from all site types, and dot line indicates contribution from each site type.

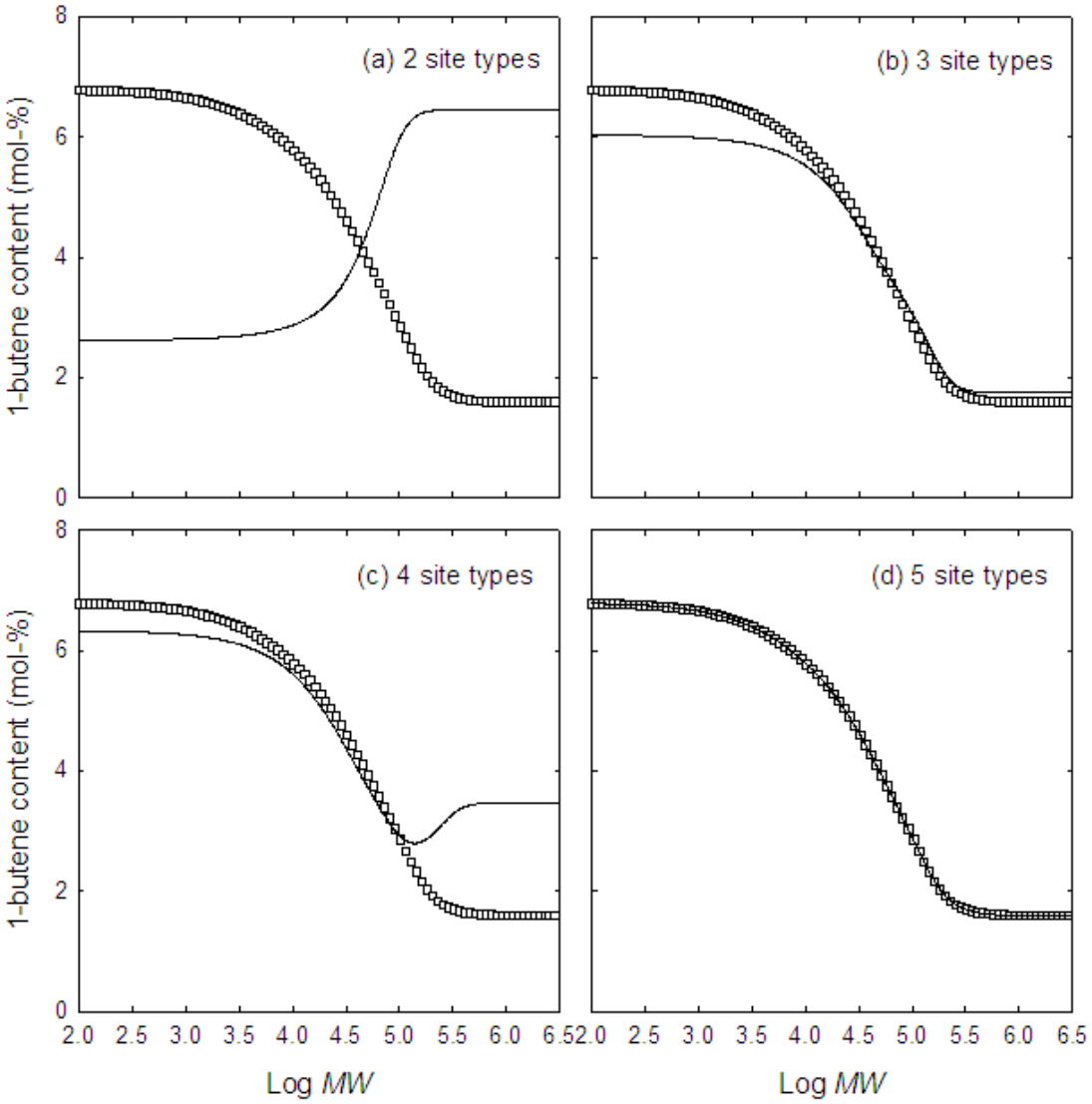

Figure 7. The relationship between MW and CC obtained from deconvolution of MWD + CCD information of the model ethylene/1-butene copolymer using a different number of site types: (a) 2, (b) 3, (c) 4, and (d) 5. Symbol (□) is the simulation data. Solid line indicates the deconvolution results from all site types.

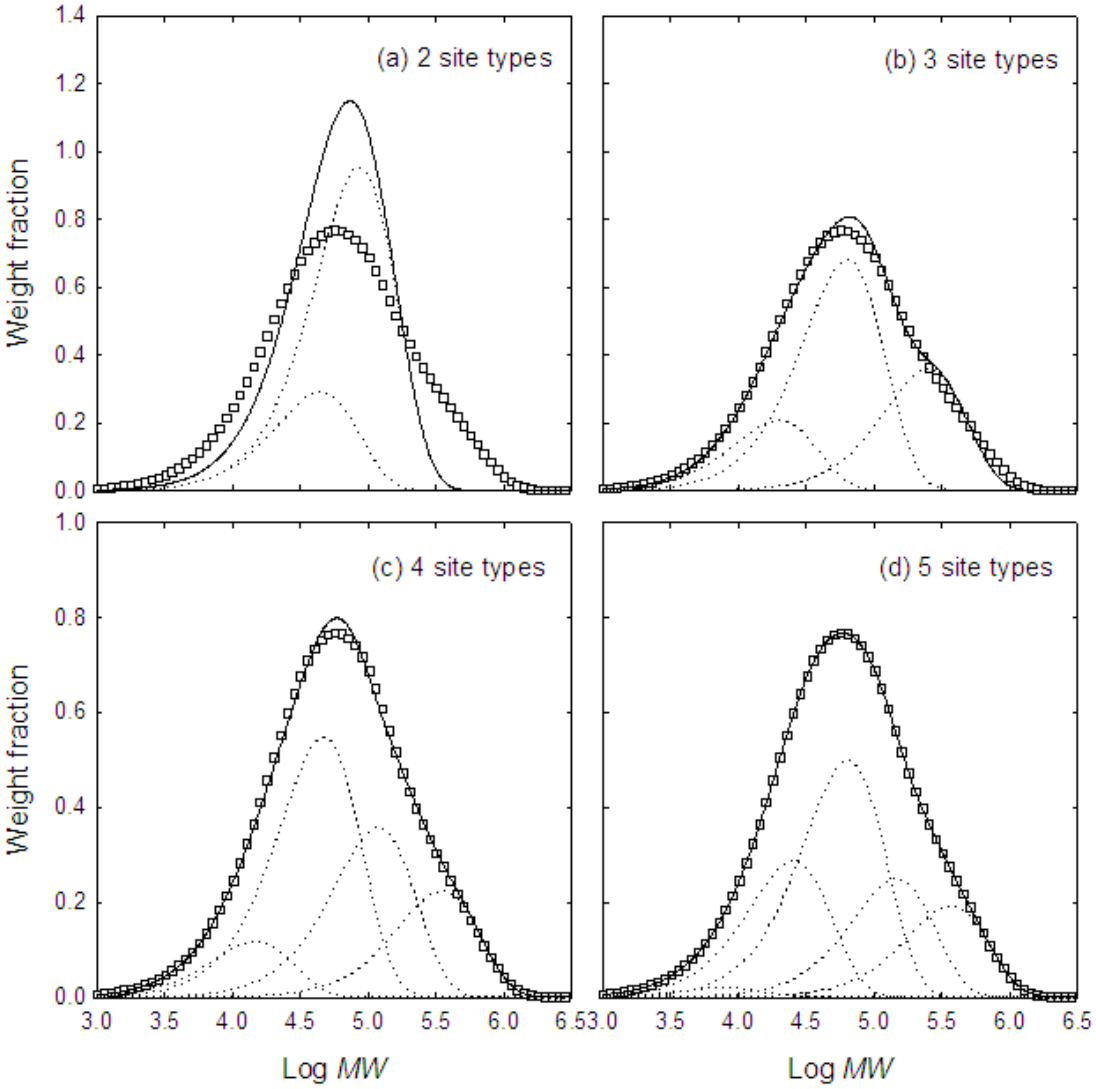

Figure 8. MWD obtained from deconvolution of MWD×CC + CCD information of the model ethylene/1-butene copolymer using a different number of site types: (a) 2, (b) 3, (c) 4, and (d) 5. Symbol (□) is the simulation data, solid line indicates the deconvolution results from all site types, and dot line indicates contribution from each site type.

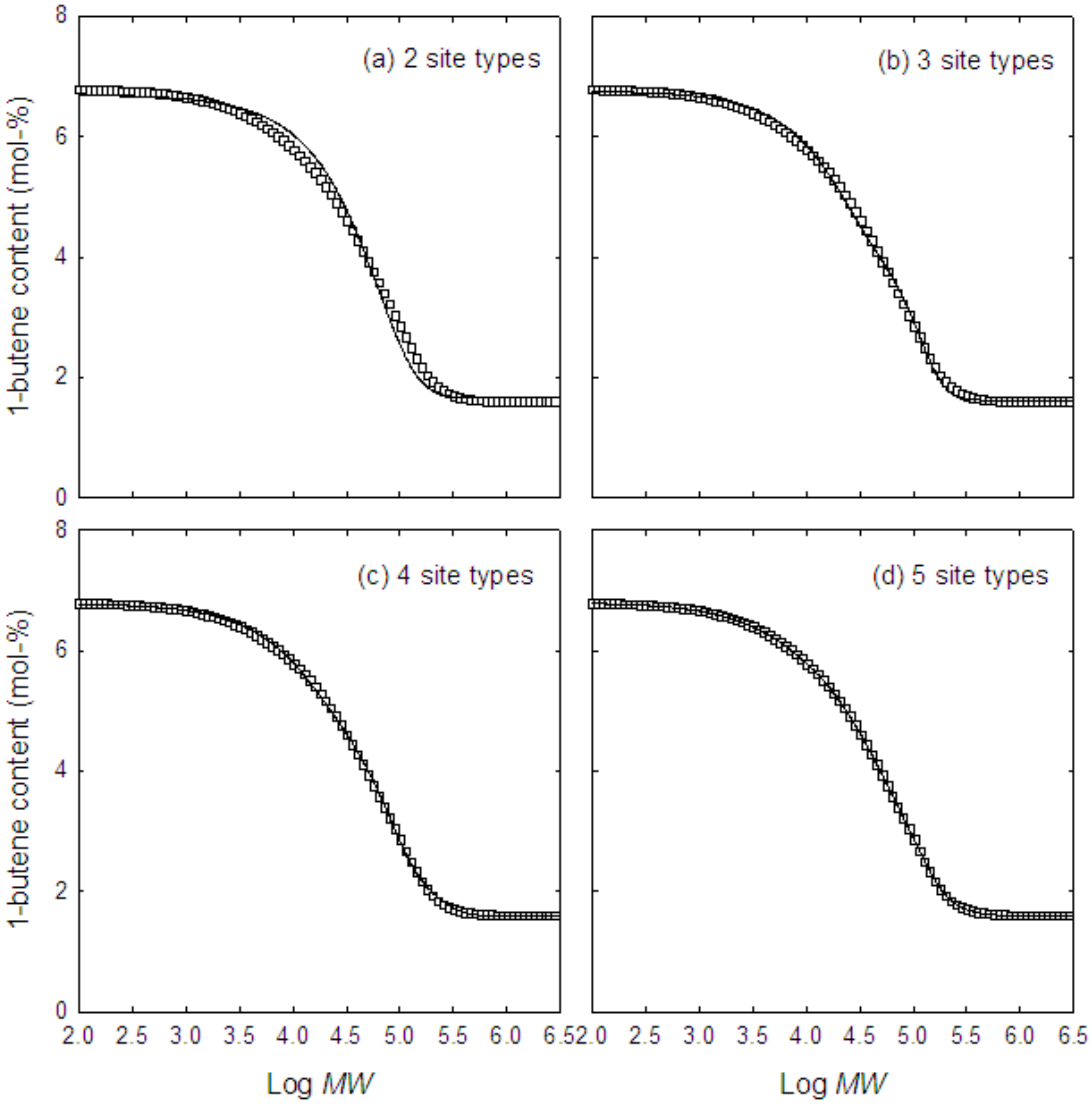

Figure 9. Relationship between MW and CC obtained from deconvolution of MWD×CC + CCD information of the model ethylene/1-butene copolymer using a different number of site types: (a) 2, (b) 3, (c) 4, and (d) 5. Symbol (□) is the simulation data. Solid line indicates the deconvolution results from all site types.

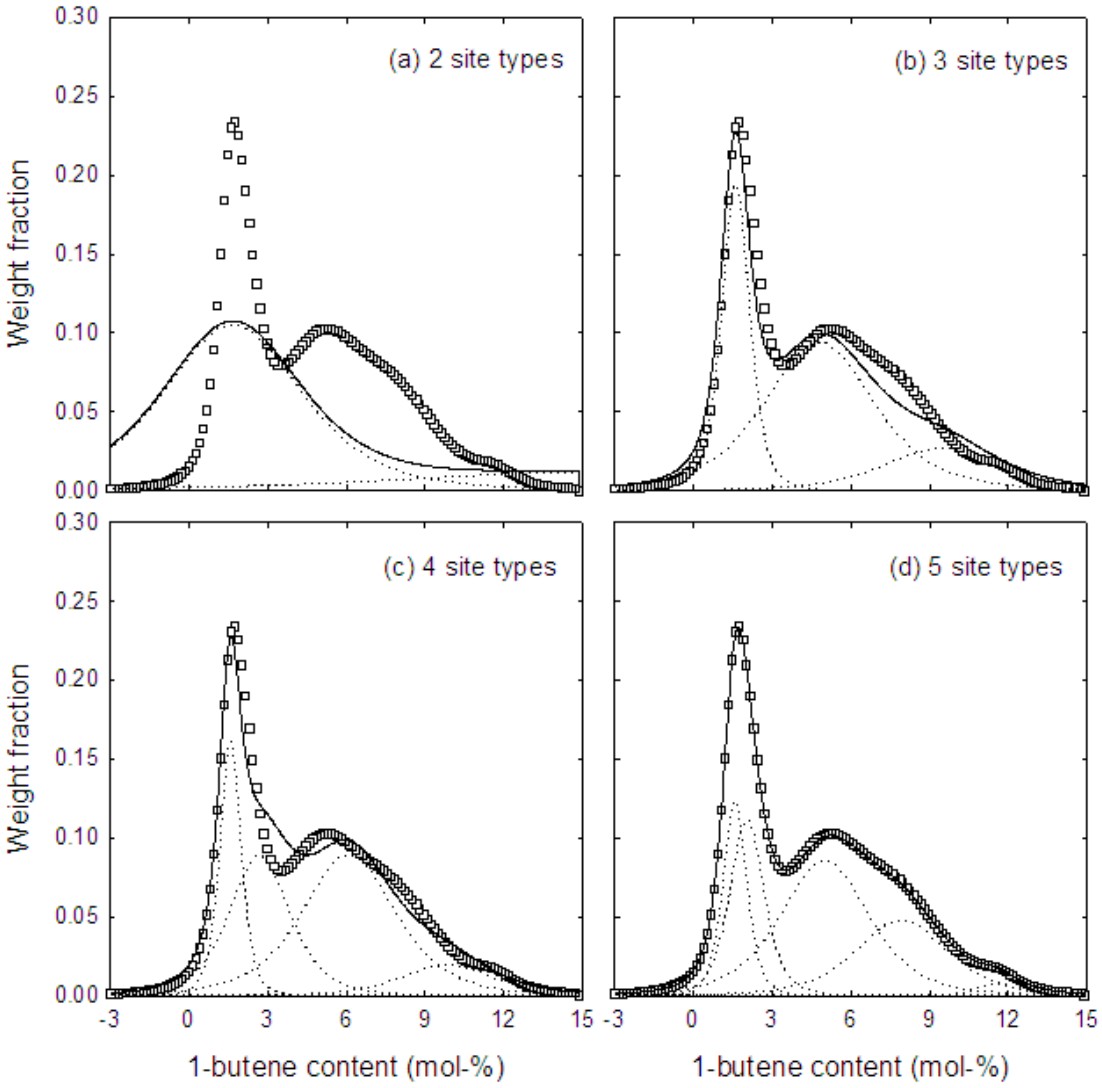

Figure 10. CCD obtained from deconvolution of MWD×CC + CCD information of the model ethylene/1-butene copolymer using a different number of site types: (a) 2, (b) 3, (c) 4, and (d) 5. Symbol (□) is the simulation data, solid line indicates the deconvolution results from all site types, and dot line indicates contribution from each site type.

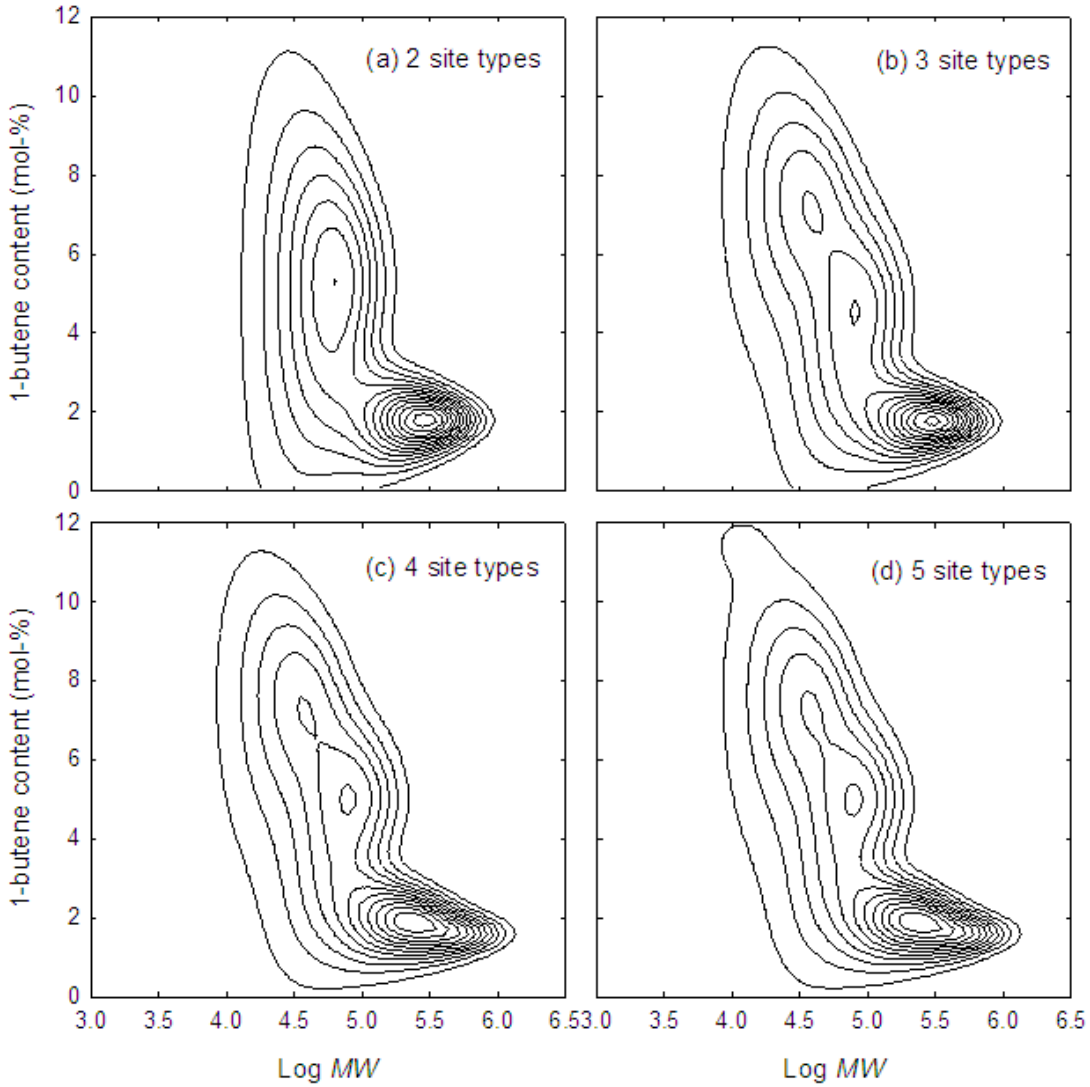

Figure 11. MWD×CCD contour plot obtained from deconvolution of MWD×CCD information of the model ethylene/1-butene copolymer using a different number of site types: (a) 2, (b) 3, (c) 4, and (d) 5.

Supplementary documents

Table S1. Summary of estimated mass fraction and kinetic parameters of each site type obtained from the simultaneous deconvolution of MWD×CC information using a different number of site types: (a) 2, (b) 3, (c) 4, and (d) 5.

Parameters	Site type				
	1	2	3	4	5
2 site types					
m	0.0330	0.9670			
$\overline{F_1}$	0.0000	0.9836			
β	0.0736	0.0384			
M_n	22,461	35,612			
3 site types					
m	0.1520	0.5579	0.2901		
$\overline{F_1}$	0.9006	0.9523	0.9838		
β	0.0819	0.0564	0.0291		
M_n	10,227	31,484	124,133		
4 site types					
m	0.0856	0.4475	0.2816	0.1854	
$\overline{F_1}$	0.8963	0.9400	0.9727	0.9841	
β	0.0868	0.0668	0.0457	0.0234	
M_n	7,687	23,112	58,452	173,082	
5 site types					
m	0.0161	0.2293	0.4006	0.2000	0.1540
$\overline{F_1}$	0.8848	0.9207	0.9500	0.9795	0.9841
β	0.0900	0.0736	0.0564	0.0384	0.0196
M_n	3,931	12,683	31,972	72,803	181,003

Table S2. Summary of estimated mass fraction and kinetic parameters of each site type obtained from the simultaneous deconvolution of MWD + CCD information using a different number of site types: (a) 2, (b) 3, (c) 4, and (d) 5.

Parameters	Site type				
	1	2	3	4	5
2 site types					
m	0.5560	0.4440			
$\overline{F_1}$	0.9807	0.9355			
β	0.1376	1.7702			
M_n	20,017	89,199			
3 site types					
m	0.2647	0.4874	0.2479		
$\overline{F_1}$	0.9253	0.9572	0.9824		
β	0.3513	1.3700	0.2390		
M_n	12,441	37,188	142,511		
4 site types					
m	0.1616	0.3578	0.3035	0.1771	
$\overline{F_1}$	0.9148	0.9419	0.9824	0.9654	
β	0.2370	0.5529	0.1236	3.1462	
M_n	10,122	24,824	56,481	173,974	
5 site types					
m	0.0158	0.2297	0.4003	0.2002	0.1539
$\overline{F_1}$	0.8838	0.9208	0.9500	0.9795	0.9841
β	0.0143	0.2537	0.6423	0.2289	0.2728
M_n	3,931	12,683	31,972	72,803	181,003

Table S3. Summary of estimated mass fraction and kinetic parameters of each site type obtained from the simultaneous deconvolution of MWD×CC +CCD information using a different number of site types: (a) 2, (b) 3, (c) 4, and (d) 5.

Parameters	Site type				
	1	2	3	4	5
2 site types					
m	0.2340	0.7660			
$\overline{F_1}$	0.8479	0.9833			
β	7.0223	2.2261			
M_n	22,296	42,981			
3 site types					
m	0.1666	0.5462	0.2871		
$\overline{F_1}$	0.9053	0.9520	0.9838		
β	0.3247	0.9727	0.2667		
M_n	9,867	31,432	125,478		
4 site types					
m	0.0946	0.4396	0.2862	0.1796	
$\overline{F_1}$	0.9019	0.9392	0.9732	0.9841	
β	0.1519	0.5069	0.5800	0.2104	
M_n	7,451	23,245	58,550	173,067	
5 site types					
m	0.0159	0.2296	0.4004	0.2002	0.1539
$\overline{F_1}$	0.8841	0.9207	0.9500	0.9795	0.9841
β	0.0142	0.2530	0.6401	0.2287	0.2724
M_n	3,932	12,682	31,972	72,803	181,003

Table S4. Summary of estimated mass fraction and kinetic parameters of each site type obtained from the simultaneous deconvolution of MWD×CCD information using a different number of site types: (a) 2, (b) 3, (c) 4, and (d) 5.

Parameters	Site type				
	1	2	3	4	5
2 site types					
m	0.6830	0.3170			
$\overline{F_1}$	0.9467	0.9822			
β	1.1526	0.3214			
M_n	24,946	116,378			
3 site types					
m	0.2386	0.4737	0.2878		
$\overline{F_1}$	0.9225	0.9537	0.9824		
β	0.2841	0.9722	0.2793		
M_n	12,112	32,666	120,341		
4 site types					
m	0.2399	0.4065	0.2002	0.1534	
$\overline{F_1}$	0.9205	0.9499	0.9795	0.9841	
β	0.2754	0.6665	0.2290	0.2744	
M_n	12,281	32,042	73,290	181,671	
5 site types					
m	0.0160	0.2300	0.4000	0.2000	0.1540
$\overline{F_1}$	0.8838	0.9208	0.9500	0.9795	0.9841
β	0.0146	0.2541	0.6428	0.2284	0.2729
M_n	3,960	12,700	32,000	72,800	181,000

Text for the Table of Contents

Four simultaneous deconvolution strategies based on different microstructural information of ethylene/1-olefin copolymers were investigated. Deconvolution based on complete bivariate distribution of molecular weight and chemical composition was found to accurately identify the number of site type and provide best estimated mass fraction and kinetic parameters of each site type.

Graphic for the Table of Contents (Color)

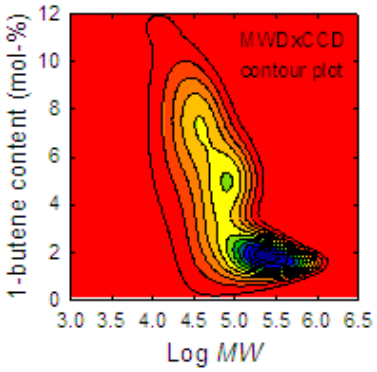

Graphic for Summary (BW)